iScience

CellPress
OPEN ACCESS

Article

Neuroblasts contribute to oligodendrocytes generation upon demyelination in the adult mouse brain

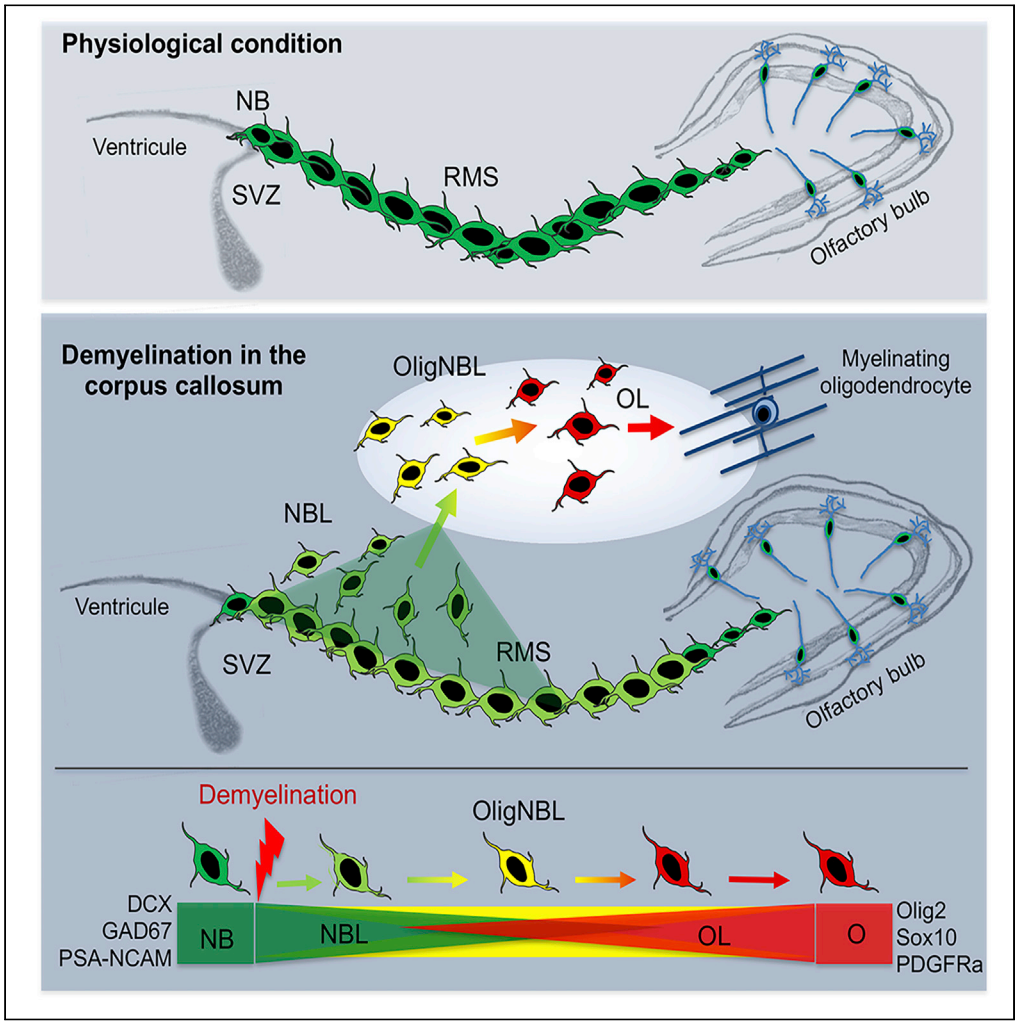

Bilal El Waly, Claire Bertet, Mathilde Paris, ..., Karine Magalon, Myriam Cayre, Pascale Durbec

pascale.durbec@univ-amu.fr

Highlights

NB can contribute to myelin repair by converting into oligodendrocytes

NB fate conversion occurs gradually, through formation of an intermediate cell type

NB fate conversion does not involve reversion toward a pluripotent state

NB fate conversion seems to involve EMT-related mechanisms and metabolic changes

El Waly et al., iScience 25, 105102
October 21, 2022
https://doi.org/10.1016/j.isci.2022.105102

iScience

CellPress
OPEN ACCESS

Article

Neuroblasts contribute to oligodendrocytes generation upon demyelination in the adult mouse brain

Bilal El Waly,[1,4] Claire Bertet,[1,4] Mathilde Paris,[1,2] Marie Falque,[1] Pierre Milpied,[3] Karine Magalon,[1] Myriam Cayre,[1] and Pascale Durbec[1,5,*]

SUMMARY

After demyelinating insult, the neuronal progenitors of the adult mouse sub-ventricular zone (SVZ) called neuroblasts convert into oligodendrocytes that participate to the remyelination process. We use this rare example of spontaneous fate conversion to identify the molecular mechanisms governing these processes. Using *in vivo* cell lineage and single cell RNA-sequencing, we demonstrate that SVZ neuroblasts fate conversion proceeds through formation of a non-proliferating transient cellular state co-expressing markers of both neuronal and oligodendrocyte identities. Transition between the two identities starts immediately after demyelination and occurs gradually, by a stepwise upregulation/downregulation of key TFs and chromatin modifiers. Each step of this fate conversion involves fine adjustments of the transcription and translation machineries as well as tight regulation of metabolism and migratory behaviors. Together, these data constitute the first in-depth analysis of a spontaneous cell fate conversion in the adult mammalian CNS.

INTRODUCTION

Understanding how cellular plasticity contributes to tissue regeneration is a fundamental question in biology and a major goal of regenerative medicine. In this context, it is crucial to identify the sequence of events specifying particular cell types and to determine how these processes are disturbed when cells change fate. Acquisition of cell identity has often been described as a unidirectional route in which each cell follows a single differentiation pathway toward a specific differentiated fate. Waddington has conceptualized this idea through his epigenetic landscape model, by depicting differentiating cells as balls passively rolling downhill through a landscape of bifurcating valleys, each representing a possible cell fate (Waddington, 1968). A cell becomes terminally differentiated when it reaches the foot of the hill. This model implies that once a cell enters one of the sub-valleys, it is restricted in its upcoming fate decisions by the path it has taken and it thus gradually looses the potential to give rise to progenies outside of its lineage (Moris et al., 2016). This linear vision has been revised over the past years. It has indeed become clear that cell fate acquisition occurs in a more discontinuous and stochastic way, with environmental cues modulating the probability of fate transition events (Moris et al., 2016; Sieweke, 2015). Consistent with this, numerous studies have shown that lineage-committed cells can display remarkable plasticity and can be fate converted either by manipulation or spontaneously after injury. Such changes usually arise in situations of tissue damage and their associated regeneration (reviewed in Jessen et al., 2015).

Cell fate conversion can proceed either directly or through dedifferentiation, a process of lineage reversion during which differentiated cells acquire properties of more immature cells within the same lineage. Dedifferentiation can be induced by expression of the Oct4, Sox2, Klf4 and c-Myc (OSKM) genes, which lead to formation of induced pluripotent stem cells (iPSCs) that can in turn be differentiated into required cell types (Takahashi and Yamanaka, 2016). Direct fate conversion can be triggered by expression of lineage-specific transcription factors (TFs). *In vitro*, this approach has been used to convert skin fibroblasts into other somatic cell types including neurons, oligodendrocytes, cardiomyocytes or blood progenitor cells (reviewed in (Chin, 2014)). It has also successfully been used *in vivo*, notably to induce conversion of astrocytes into functional neurons after brain lesion (Berninger et al., 2007; Heinrich et al., 2010; Heins et al., 2002). Although expression of key TFs is sufficient to induce direct fate conversion, recent lines of evidence

[1]Aix Marseille Univ, CNRS, IBDM, Marseille, France

[2]Institut de Génomique Fonctionnelle de Lyon (IGFL), École Normale Supérieure de Lyon, Lyon, France

[3]Aix Marseille Univ, CNRS, INSERM, CIML, Marseille, France

[4]These authors contributed equally

[5]Lead contact

*Correspondence: pascale.durbec@univ-amu.fr

https://doi.org/10.1016/j.isci.2022.105102

suggest that environmental factors and cellular state, such as cell proliferation rate (Halley-Stott et al., 2014; Ruiz et al., 2011) or metabolic status (Zhang et al., 2012) significantly influence the efficiency of these forced conversions (For review see (Gascon et al., 2016). For instance, the balance between glycolysis and oxidative phosphorylation (OXPHOS) has a direct impact on neuron to glia fate conversion, because neurons rely on OXPHOS whereas glial cells rather utilize anaerobic glycolysis and beta-oxidation (McKay et al., 1983; Tsacopoulos and Magistretti, 1996).

Spontaneous fate conversions are rare events that have been observed during development or after injury in both vertebrates and invertebrates (Jopling et al., 2011). In contrast to induced fate conversions, the molecular mechanisms controlling these events are still poorly understood. Several studies have shown that they require a dedifferentiation step through expression of OSKM genes and in most cases cell divisions (Gadye et al., 2017; Kagias et al., 2012; Lin et al., 2017), but notable differences have been observed depending on the tissue, type of injury or cell state (Gascon et al., 2017; Jopling et al., 2011; Tata and Rajagopal, 2016). In particular, it is still unclear whether these processes can occur directly, without reversion to an immature state.

Spontaneous remyelination of the CNS, which occurs in humans and rodents, is a good model system to study spontaneous fate conversion. This regenerative process is particularly efficient in the adult mouse brain, where it involves neural stem cells (NSCs) of the sub-ventricular zone (SVZ) (Brousse et al., 2015; El Waly et al., 2018; Jablonska et al., 2010; Xing et al., 2014). In physiological conditions, SVZ NSCs generate transit-amplifying progenitors, the neural precursor cells (NPC also called C-Cell), which give rise to GAD67-expressing neuroblasts (NB) and, to a lesser extent, to Olig2-expressing oligodendrocyte progenitor cells (OPCs), the precursors of myelin-forming cells (Capilla-Gonzalez et al., 2013). GAD67^{+} NB migrate along the rostral migratory stream (RMS) toward the olfactory bulbs where they differentiate into interneurons. This migration is a cooperative process during which NB are organized in chains and tightly linked by gap or adherens junctions (Lois and Alvarez-Buylla, 1994; Lois et al., 1996; Wichterle et al., 1997). Following demyelination, SVZ NSCs increase their production of Olig2^{+} OPC, which migrate radially toward the corpus callosum and the cortex (Menn et al., 2006). Here, they differentiate into myelinating oligodendrocytes and significantly contribute to myelin regeneration (Menn et al., 2006). Interestingly, a subset of GAD67^{+} NB also participates to this myelin repair process by spontaneously changing fate (El Waly et al., 2018; Jablonska et al., 2010): they start expressing markers of the oligodendrocyte lineage such as Olig2, leave the RMS and ectopically migrate as isolated cells toward lesions, where they produce new myelinating oligodendrocytes (El Waly et al., 2018; Jablonska et al., 2010). The contribution of neuronal progenitors to oligodendrocytes formation during remyelination has also been reported in the hippocampus (Klein et al., 2020). However, the molecular mechanisms controlling this rare example of *in vivo* spontaneous cell fate conversion remain unknown.

Here we demonstrate that SVZ NB lineage plasticity is systematically induced on demyelinating conditions and significantly contributes to the repair process. Using single cell transcriptomic approaches, we provide evidence that this spontaneous neuron-to-oligodendrocyte fate conversion proceeds through formation of a non-proliferating transient intermediate state, during which cells concomitantly express neuronal and oligodendrocytic markers. The fate change starts immediately after demyelination and occurs gradually, by an upregulation of oligodendrocyte genes and a concomitant downregulation of neuronal genes. It involves fine adjustments of the transcription and translation machineries and is accompanied by adjustments in the metabolic status of the cells. The change in migratory behavior of converting cells seems to be controlled by epithelial to mesenchymal transition (EMT)-related mechanisms. This work represents the first description of a spontaneous cell fate conversion involving formation of an intermediate cell type co-expressing two distinct genetic programs.

RESULTS

SVZ NB exhibit lineage plasticity after brain demyelination

Following Lysolecithin (LPC)-induced demyelination of brain corpus callosum (CC), GAD67-GFP^{+} SVZ NB modify their molecular properties and migratory path (Cayre et al., 2013; Jablonska et al., 2010) (Figures 1A and 1B). They start expressing markers of the oligodendrocyte lineage such as Olig2 (Figures 1B and 1C). They leave the RMS (Cayre et al., 2013) and accumulate in demyelinating lesions, where they differentiate into oligodendrocytes.

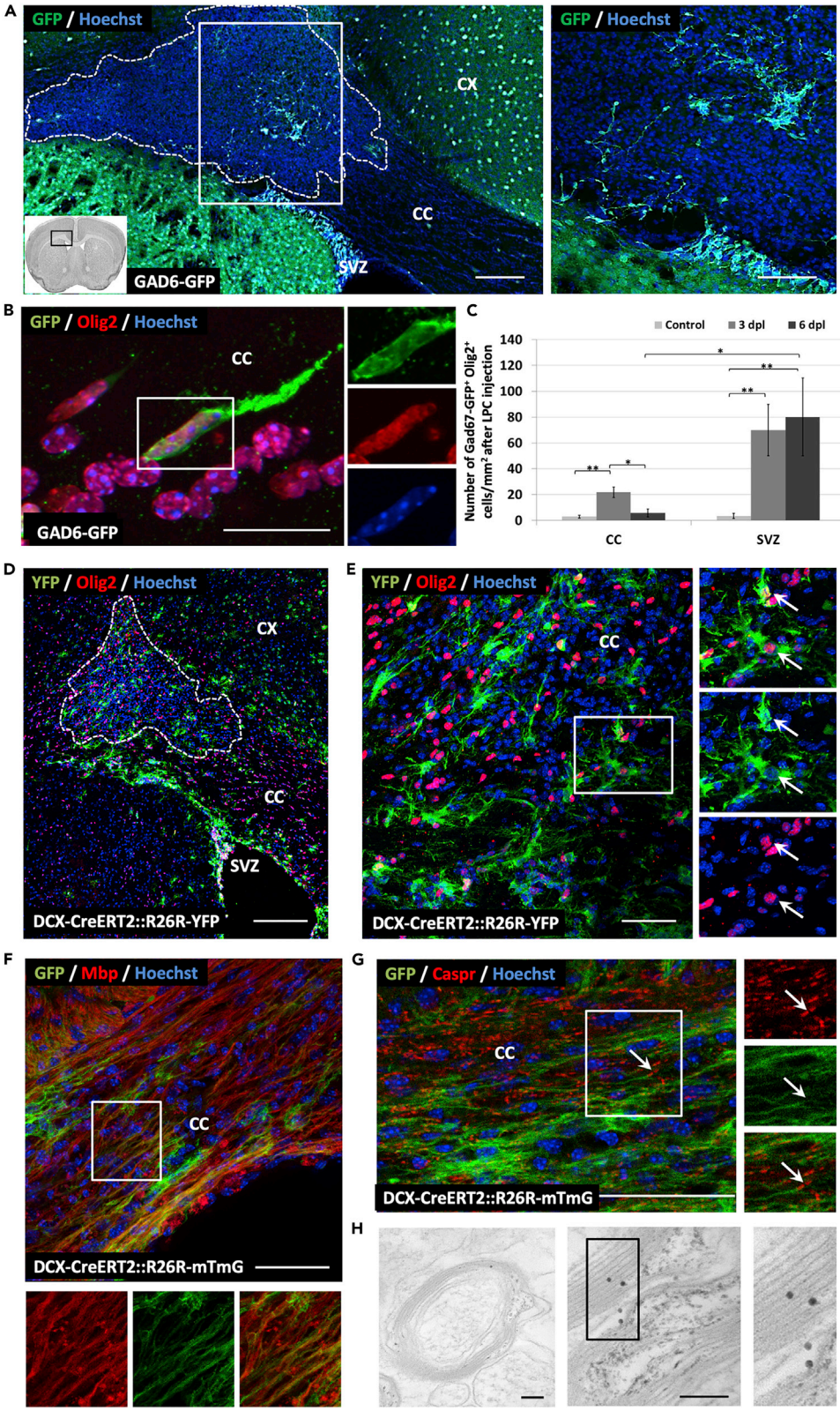
A
GFP / Hoechst
CX
CC
SVZ
GAD6-GFP
GFP / Hoechst
B
GFP / Olig2 / Hoechst
CC
GAD6-GFP
C
Control
3 dpl
6 dpl
Number of Gad67-GFP+ Olig2+ cells/mm2 after LPC injection
140
120
100
80
60
40
20
0
*
**
**
**
*
CC
SVZ
D
YFP / Olig2 / Hoechst
CX
CC
SVZ
DCX-CreERT2::R26R-YFP
E
YFP / Olig2 / Hoechst
CC
DCX-CreERT2::R26R-YFP
F
GFP / Mbp / Hoechst
CC
DCX-CreERT2::R26R-mTmG
G
GFP / Caspr / Hoechst
CC
DCX-CreERT2::R26R-mTmG
H

Figure 1. Lineage plasticity of SVZ neuroblasts after LPC induced demyelination

(A–C) LPC-induced demyelination of GAD67-GFP mouse, 6 days after injection. (A) GFP^+ NB (green) ectopically migrate from the RMS toward the lesion site in the CC (dashed line). Higher magnification: GFP^+ NB exiting the RMS. (B) Some GFP^+ NB start expressing oligodendrocyte markers such as Olig2 (red). (C) Density of GAD67-GFP^+ $Olig2^+$ cells in the CC and SVZ, 3 and 6 dpi. Error bars: mean ± SEM *$p < 0.05$, **$p < 0.01$; Mann-Whitney test (n= 5 mice).

(D and E) LPC-induced demyelination of DCX-CreERT2:YFP mouse. 7 days after LPC injection, YFP^+ NB are identified in the lesion (dashed line) and some of them express the oligodendrocyte marker Olig2 (red).

(F–H) LPC-induced demyelination of DCX-CreERT2:mTmG mouse. 3 weeks after LPC injection at the site of the lesion, GFP^+ cells adopt a complex morphology and express the mature oligodendrocyte marker MBP (red in F) and GFP^+ segments are flanked by Caspr staining indicating paranodal organization. (H) Electron micrograph showing GFP immunogold-labeled myelin sheaths. The presence of gold beads within compact myelin sheaths surrounding axons an attests for the differentiation of GFP^+ NB into myelinating oligodendrocytes. Scale bars: 200 μm in A and D, 20 μm in B, 50 μm in E to G and 150 nm in H. SVZ: sub-ventricular zone, CC: corpus callosum, CX: cortex, LV: lateral ventricle.

To quantify the contribution of SVZ NB to the repair process, we performed lineage-tracing experiments, by crossing DCX-CreERT2 mice to R26R-YFP mice (Srinivas et al., 2001). In the progeny of these mice, tamoxifen induces permanent and robust YFP labeling of NB. To estimate the labeling efficiency of this strategy, we counted the number of YFP^+ DCX^-expressing NB in the SVZ/RMS of adult mice, after 5 consecutive days of tamoxifen exposure. Around 28% ± 2% of DCX^+ NB were labeled with YFP, thus suggesting that on average, this strategy allows us to label and follow one-third of the SVZ NB population (n = 3 mice). Consistent with previous results, seven days post-LPC injection, numerous YFP^+ cells were observed in the demyelinated CC and at the lesion site (Figures 1D and 1E). Among these YFP^+ cells, 38% ± 4 cells were $Olig2^+$, indicating that after leaving the RMS, almost half of lineage-traced NB start converting into oligodendrocytes (Figure 1E). More importantly, at this stage, YFP^+ $Olig2^+$ cells represented 8% ± 1% of the total $Olig2^+$ population in the lesion (n = 3 mice). Because our tracing strategy labels at best one-third of the NB population, we concluded that up to 25% of $Olig2^+$ cells in the lesion could be converted SVZ NB.

Demyelinating lesions also induce mobilization of parenchymal OPC (pOPC). To rule out the hypothesis that pOPC can convert into NB and contribute to the YFP^+ $Olig2^+$ cell population observed in the lesion, we performed lineage-tracing experiments of pOPC, by crossing PDGFRa-CreERT2 mice (Rivers et al., 2008) to R26R-YFP mice (Srinivas et al., 2001). After LPC-induced demyelination, none of the YFP^+ cells OPC-derived expressed the specific neuronal marker DCX (Figure S1). Thus, the YFP^+ $Olig2^+$ solely correspond to converted NB.

To determine whether converted NB efficiently undergo terminal differentiation and produce myelin sheaths, we next crossed pDCX-CreERT2 with the mTmG reporter mouse line, another Rosa26-based reporter, which on Cre-mediated recombination expresses a myristylated GFP, thus enabling to visualize myelin segments.

Three weeks after LPC injection, we observed some GFP^+ cells in the CC exhibiting typical OLG morphology (Figure 1F). These cells displayed a typical shape of myelinating oligodendrocytes with GFP^+ MBP^+ long segments (Figure 1F) decorated with Caspr/Paranodin (Figure 1G), which was reminiscent of myelin segments with functional nodes of Ranvier. Electron microscopy coupled with GFP immunogold labeling unequivocally demonstrated that these converted NB form compact myelin sheaths around axons (Figure 1H).

Finally, to test the universality of this fate conversion, we used another model of demyelination, cuprizone intoxication, which induces apoptosis of mature oligodendrocytes, leading to general and robust brain demyelination. Using both GAD67-GFP mice and cell lineage tracing (DCX-CreERT2 mice), we showed that similarly to LPC injection, cuprizone-induced demyelination induces SVZ NB fate conversion (Figure S2).

Altogether, these results indicate that following demyelination, SVZ NB significantly contribute to the repair process by changing fate and converting into oligodendrocytes.

Transcriptome analysis of five cell populations representing the continuum of SVZ NB fate conversion

To unravel the molecular mechanisms underlying SVZ NB fate conversion, we used the LPC paradigm and performed single cell RNA-sequencing from five cell populations representing distinct states of the

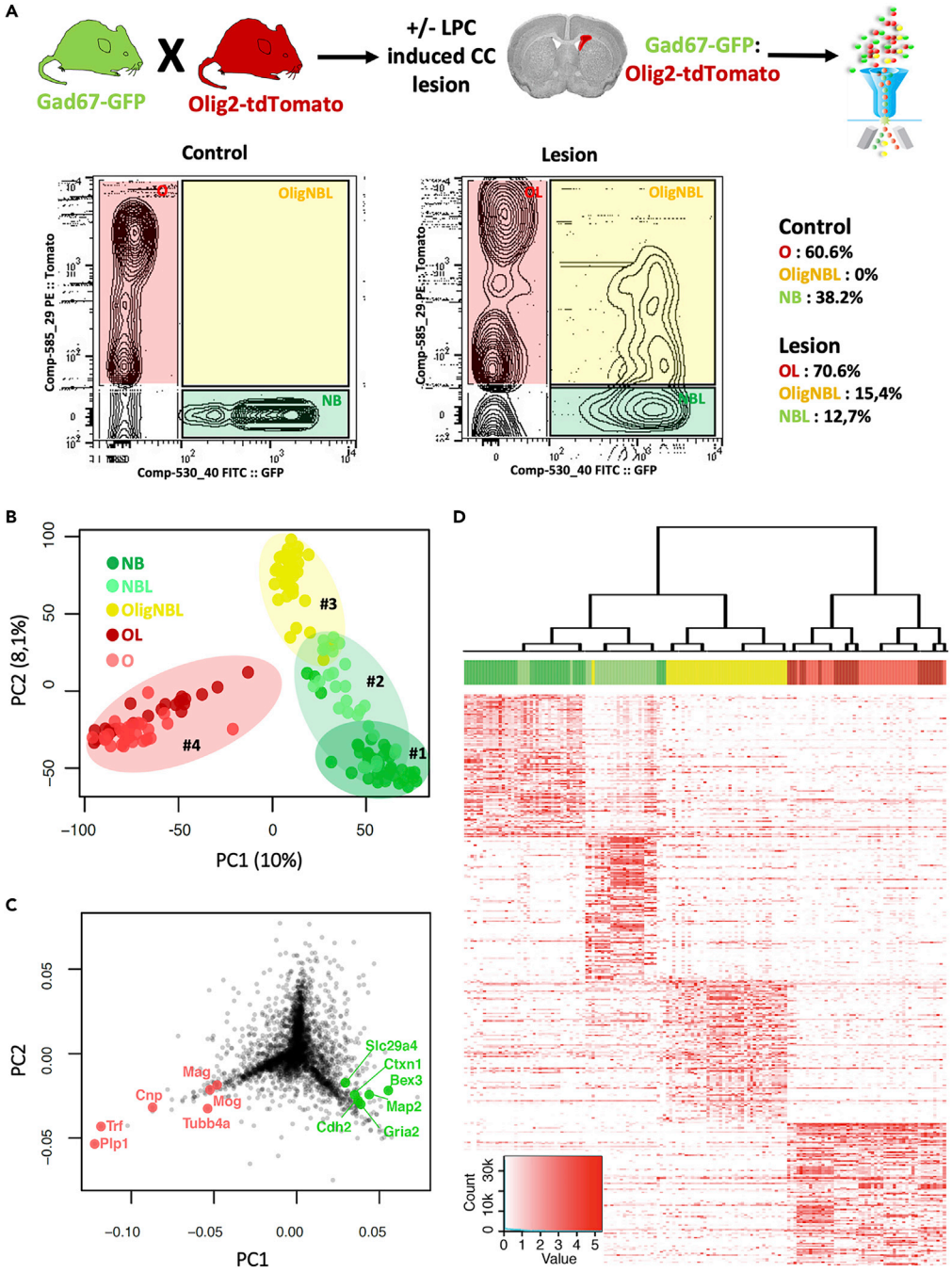

Figure 2. Single cell RNA-seq of 155 cells from five populations representing the continuum from neuroblast to oligodendrocyte during demyelination-induced fate conversion

(A) FACS strategy to isolate the 5 cell populations. All cells derive from GAD67-GFP:Olig2-tdTomato mice. Neuroblasts (GFP^+, referred to NB and NBL in control and lesion mice respectively) and oligodendrocytes ($Tomato^+$, referred to O and OL in control and lesioned mice, respectively) were purified from the SVZ and CC (n = 5 mice per group). In lesioned mice (6 days after LPC injection), a double-positive population (GFP^+ $Tomato^+$, referred to OligNBL) appeared and was also purified for RNA-sequencing.

(B) PCA of 155 high-quality single cell RNA-seq transcriptomes separated the cells into 4 clusters corresponding to their population of origin: #1 NB, #2 NBL, #3 OligNBL and #4 O + OL.

Figure 2. *Continued*
(C) Projection of gene coordinates on the PCA. As expected, NB (cluster #1) and O + OL (cluster #4) are associated with expression of neuronal (green dots) and oligodendrocyte genes (red dots), respectively.
(D) Biclustering using the top 100 genes specifically enriched in each cell population cluster. Cells are shown in columns and genes in rows.

continuum of this fate conversion: GAD67$^+$ control neuroblasts (NB), GAD67$^+$ neuroblasts after lesion (NBL), GAD67$^+$ Olig2$^+$ cells after lesion (OligNBL), Olig2$^+$ oligodendrocytes after lesion (OL) and Olig2$^+$ control oligodendrocytes (O) (Figure 2).

To FACS-isolate these cell populations, we generated GAD67-GFP:Olig2-tdTomato double transgenic mice in which NB and NBL (GAD67$^+$) are labeled in green, O and OL (Olig2$^+$) in red and OligNBL (GAD67$^+$, Olig2$^+$) in yellow (STAR Methods, Figures 2A and S3). NBL, OligNBL and OL single cells were dissociated from dissected SVZ and CC from demyelinated mice (8–10 weeks old, n = 5 mice) 6 days after LPC injection, during the peak of cell mobilization in the SVZ. Control NB and O single cells were collected from PBS injected mice (8–10 weeks old, n = 5 mice). In these mice, no GFP$^+$ Tomato$^+$ positive cells (OligNBL) were observed after FACS sorting (Figure 2A). A total of 184 RNA-sequencing libraries were prepared using Smart-Seq2 technology and were sequenced at an average depth of 8.8 million reads per cell. We excluded low quality cells based on a threshold for number and percentage of reads mapping to the transcriptome (>200,000 reads per cell, >20% of mapping rate, Figure S4A). 155 cells passed this quality control: 37 NB, 27 NBL, 40 OligNBL, 22 OL and 29 O. As expected, gene expression levels were more highly correlated within cell types than between cell types (Spearman correlation ~0.37 within cells of each cell type).

Principal component analysis (PCA) on the 155 high-quality single cells identified 4 clusters generally corresponding to the expected cell populations (Figure 2B): #1 NB (green), #2 NBL (light green), #3 OligNBL (yellow), #4 OL and O (dark red and red), with groups #1 and #4 localized at the two extremities of PC1 axis. We checked that this signal was not driven by confounding factors such as library preparation or differences in read count (the latter is shown in Figure S4C). Close examination of the genes exhibiting the highest loadings in PC1 revealed that group #1 (enclosing NB) was associated with expression of neuronal markers such as Gria2, Map2, Bex3, Ctxn1 and Cdh2 whereas group #4 (O and OL) was associated with expression of glial markers such as Plp1, Trf, Cnp, Mog and Mag (Figure 2C). Two-way unsupervised clustering analysis using backspin (Zeisel et al., 2015) with the 1,000 most variable genes also separated the cell populations into 4 main clusters corresponding to the different cell types (Figure S4B, Table S1). As expected, the top 100 genes specifically enriched in each of the 4 cluster populations contained characteristic markers of neuronal and oligodendrocyte identities (Figure 2D and Table S2). These genes were used in subsequent meta-analyses (Figure 3). Together, these results showed that NB, NBL, OligNBL and OL/O have distinct transcriptomes that can be classified and analyzed by single cell RNA-sequencing.

NB-to-O fate conversion proceeds through formation of an intermediate cell type co-expressing neuronal and oligodendrocyte markers

SVZ NB fate conversion could proceed in two ways (Figure 3A): (1) dedifferentiation/redifferentiation involving a transient pluripotent progenitor cell or (2) conversion via an intermediate cell type carrying markers of both the donor and target cell fates. The existence of OligNBL co-expressing neuronal and oligodendrocyte markers (GAD67-GFP$^+$ Olig2$^+$ and (Jablonska et al., 2010)) supported the intermediate cell type model.

To confirm this, we first tested whether OligNBL exhibit transcriptomic similarities with the nearest common progenitors of NB and O, i.e. the neural precursor cells (NPC) and the activated neural stem cells (aNSC, Figure 3A). To do so, we conducted meta-analyses with a single-cell dataset of the adult SVZ neural stem cell lineage from the study of Dulken et al. (2017). As a control, we included in these analyses a dataset of the CNS oligodendrocyte lineage from Marques et al. (Marques et al., 2018. PCA on this *meta*-dataset using the top 400 genes defining the 4 clusters (NB, NBL, OligNBL and OL/O, Table S2 and Figure 2D) ordered all cells according to lineage identity and maturation levels (Figure 3B): aNSC and NPC (blue) clustered on one side of the first PCA axis (PC1) whereas oligodendrocytes (pink/red) segregated on the other side, in a gradient from less mature (Oligodendrocyte precursors cells, OPC) to most mature cells (Mature Oligodendrocytes, MOL6). Consistent with their expression of mature oligodendrocyte markers (Plp1, Mog and Mag,

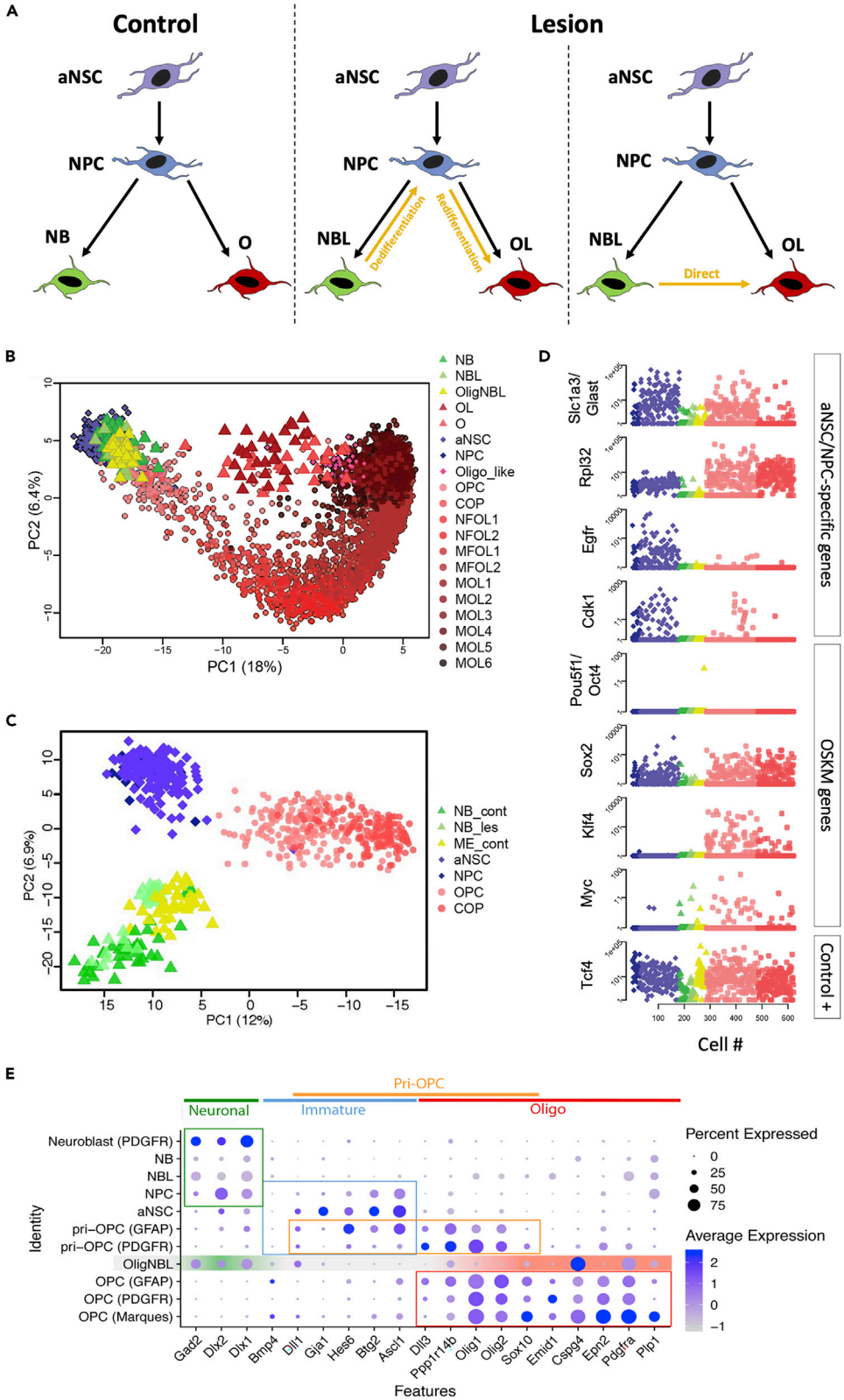
A
Control
Lesion
aNSC
NPC
NB
O
NBL
OL
Dedifferentiation
Redifferentiation
Direct
B
PC2 (6.4%)
PC1 (18%)
NB
NBL
OligNBL
OL
O
aNSC
NPC
Oligo_like
OPC
COP
NFOL1
NFOL2
MFOL1
MFOL2
MOL1
MOL2
MOL3
MOL4
MOL5
MOL6
C
PC2 (6.9%)
PC1 (12%)
NB_cont
NB_les
ME_cont
aNSC
NPC
OPC
COP
D
Slc1a3/ Glast
Rpl32
Egfr
Cdk1
Pou5f1/ Oct4
Sox2
Klf4
Myc
Tcf4
aNSC/NPC-specific genes
OSKM genes
Control +
Cell #
E
Pri-OPC
Neuronal
Immature
Oligo
Neuroblast (PDGFR)
NB
NBL
NPC
aNSC
pri–OPC (GFAP)
pri–OPC (PDGFR)
OligNBL
OPC (GFAP)
OPC (PDGFR)
OPC (Marques)
Identity
Gad2
Dlx2
Dlx1
Bmp4
Dll1
Gja1
Hes6
Btg2
Ascl1
Dll3
Ppp1r14b
Olig1
Olig2
Sox10
Emid1
Cspg4
Epn2
Pdgfra
Plp1
Features
Percent Expressed
0
25
50
75
Average Expression
2
1
0
−1

Figure 3. SVZ neuroblast fate conversion does not involve a dedifferentiation step

(A) SVZ NB fate conversion into O could either involve a dedifferentiation step into aNSC/NPC or could proceed through formation of an intermediate cell type.

(B) PCA on a *meta*-dataset of single cell RNA-seq experiments comprising our data (triangles) and datasets from *Dulken* et al. (Dulken et al., 2017) (diamond shapes) and *Marques* et al. (Marques et al., 2018) (dots), using the top 100 genes defining our 4 cell populations according to biclustering analyses. NBL (light green triangles) and OligNBL (yellow triangles) cluster between aNSC/NPC (blue diamond shapes) and OPC (red dots). O (red triangles) and OL (dark red triangles) cluster with mature oligodendrocytes.

(C) PCA using only immature cells from the *meta*-dataset shows that NBL and OligNBL cluster away from aNSC and NPC.

(D) Expression levels (TPM) of relevant markers for aNSC/NPC (GLAST/Slc1a3, Rpl32, Egfr, Cdk1) and the OSKM reprogramming set (Pou5f1/Oct4, Sox2, Klf4, Myc) in various cell populations. NBL and OligNBL do not express significant levels of these markers but express the oligodendrocyte marker Tcf4 (positive control).

(E) OligNBL harbors a unique molecular identity, distinct from pri-OPC. Dot plot of expression of select genes in 11 cell populations from a *meta*-dataset comprised 152 aNSCs and 29 NPCs from Dulken et al. (2017); our 37 NB, 27 NBL and 40 OligNBL, 1070 NB, 143 pri-OPCs-GFAP, 738 pri-OPCs-PDGFR, 90 OPCs-GFAP and 340 OPCs-PDGFR from Weng et al. (2019) and 201 OPCs from Marques et al., (2018) for a total of 2877 cells.

Figure 2C), our O/OL (red triangles) aligned with oligodendrocytes from Dulken et al. (2017) (pink diamond shapes) and clustered between OPC and mature oligodendrocytes from Marques et al., (2018) (MOL, dark red dots). As expected, NB, NBL and OligNBL clustered with immature cells, between aNSC/NPC (blue) and OPC (pink dots) (Figure 3B). To gain resolution, we conducted a second PCA using only immature cells (Figure 3C). We found that OligNBL clustered close to NB and NBL and away from aNSC/NPC, thus indicating that they do not exhibit transcriptomic similarity with aNSC/NPC. In accordance with this result, OligNBL did not express aNSC/NPC-characteristic genes (Chaker et al., 2016) such as GLAST/Slc1a3, the ribosomal protein Rpl32, the cell cycle proteins Cdk1, Ccna2 and Mik67 or EGFr (Figures 3D and Table S3). They also did not express genes from the Oct4 Sox2 Klf4 c-Myc (OSKM) reprogramming set, which induce cell dedifferentiation and pluripotency (Figure 3D and Table S3). We also confirmed that OligNBL do not resemble the embryonic primitive OPC (Pri-OPC) described by Weng et al. (2019). By using marker genes described in Weng et al. (2019) we show that OligNBL harbor a unique molecular identity compared with 10 other cell populations from a *meta*-dataset comprised aNSC and NPC from Dulken et al. (2017); our NB and NBL, Neuroblasts, pri-OPC-GFAP, pri-OPC-PDGFR, OPC-GFAP and OPC-PDGFR from Weng et al. (2019) and OPC from Marques et al., (2018) (Figure 3E). Taken together, these data suggest that SVZ NB fate conversion does not proceed through a pluripotent intermediate stage.

We next performed monocle pseudo-temporal ordering of the 5 cell populations based on the expression of 396 genes identified by Monocle as differentially expressed between the donor (NB) and target (O) cell fates of the continuum (Table S4, Figure 4A). As expected, this ordering placed NB and O/OL at opposite ends of the pseudotime axis. The O/OL cell population separated into 2 branches that did not correspond to maturation levels and/or cell cycle status. Importantly, NBL and OligNBL were ordered between NB and O/OL, suggesting that their transcriptome is intermediate between these cell types. To confirm this, we used an independent method in which we examined how expression of gene-sets that distinguish NB from O varies in the 5 cell populations of the continuum (Figure 4B). These gene-sets were generated by differential expression analyses between NB and O with the SCDE tool (Kharchenko et al., 2014) and consisted of 489 genes upregulated in NB as compared to O and 344 genes upregulated in O as compared to NB (referred to as NB-identity and O-identity genes thereafter, Table S5). We found that expression of NB-identity genes (green, Figure 4B) gradually decreased during the transitions from NB to O, whereas expression of O-identity genes (red, Figure 4B and Tables S6 and S7) gradually increased. Consistent with the results of Monocle cell ordering, OligNBL co-expressed a subset of NB-identity and O-identity genes: 26% (128/489 genes) and 18% ($6^2/_3$44 genes), respectively (Figure 4B). Furthermore, OligNBL expressed genes associated with early neuronal differentiation such as Dlx1, Dlx2 together with oligodendrocyte precursor markers such as PDGFRa and Cspg4/NG2 (Table S3), thus arguing that this cell population has a dual NB/O identity. We validated these observations by immunostaining on GAD67-GFP mice 6 days after LPC-induced focal demyelination (Figure 4C). We found that a large number of GAD67-GFP$^+$ Olig2$^+$ OligNBL in SVZ and CC co-expressed the neuronal markers Tuj1 (81% $\pm$ 4.6%) or PSA-NCAM (74% $\pm$ 3.3%). We also showed that OligNBL co-expressed early oligodendrocyte markers such as Cspg4/NG2 (87% $\pm$ 8.4%), Sox10 (72% $\pm$ 1.5%) or PDGFRa (17% $\pm$ 1.1%). Unlike NBL and OL, none of these cells were labeled with the proliferation marker EdU (injected 2h before animal sacrifice) (Figure 4D). Indeed, among EdU$^+$ proliferative cells we observed 4.5% of GFP$^+$ NBL, 61.4% of Tomato$^+$ OL, 34,1% of GFP$^-$ Tomato$^-$ but no GFP$^+$ Tomato$^+$ cells OligNBL.

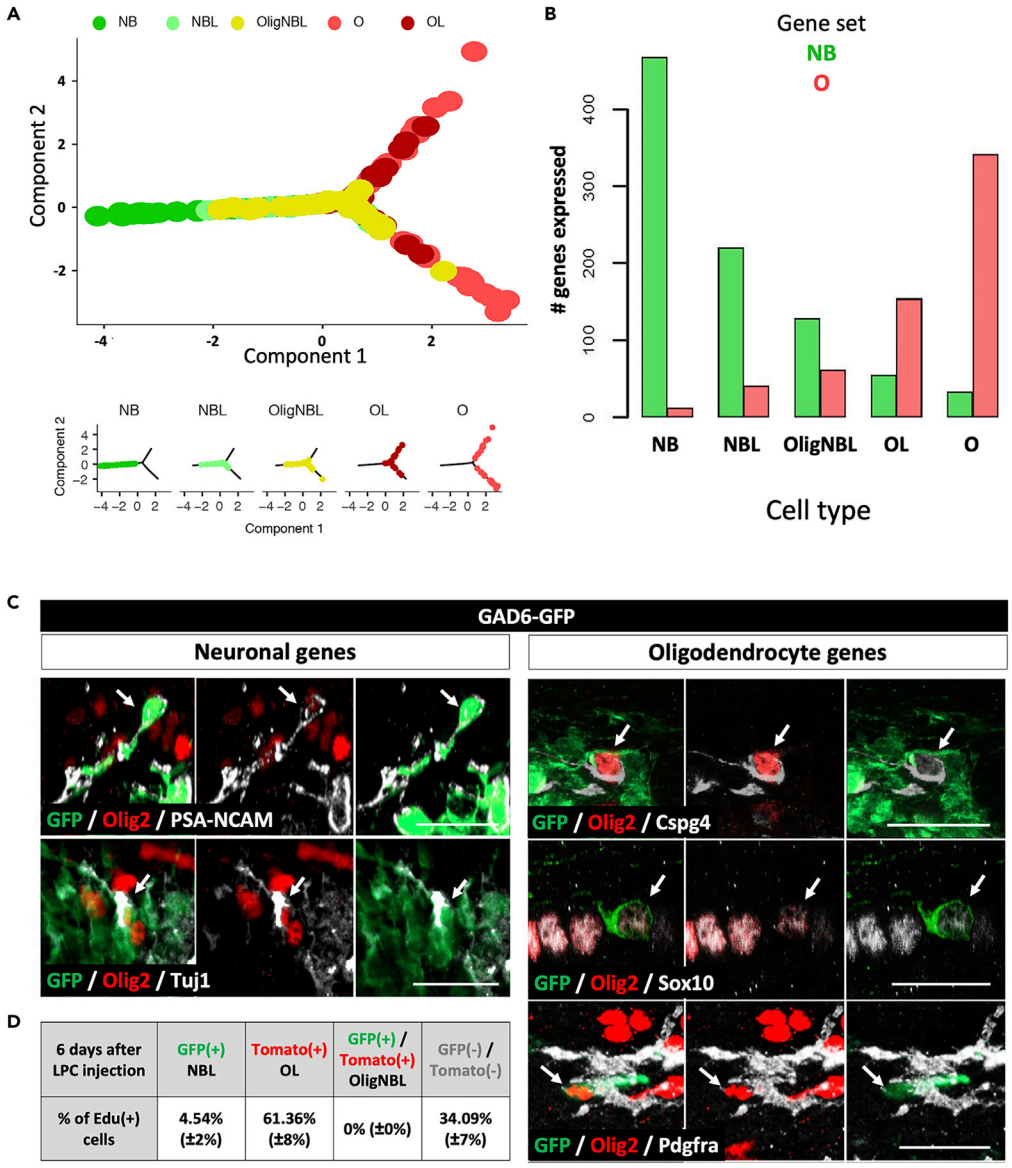

6 days after LPC injection	GFP(+) NBL	Tomato(+) OL	GFP(+) / Tomato(+) OligNBL	GFP(-) / Tomato(-)
% of Edu(+) cells	4.54% (±2%)	61.36% (±8%)	0% (±0%)	34.09% (±7%)

Figure 4. SVZ neuroblast fate conversion proceeds through formation of an intermediate cell type carrying both NB and O identities

(A) Pseudo-temporal ordering of the 5 cell populations based on the expression of 396 genes identified by Monocle as differentially expressed between NB and O. The trajectory of each cell population is illustrated below the main graph. NBL and OligNBL align between NB and O suggesting that their transcriptome is intermediate between these 2 cell types.

(B)Number of genes characterizing the NB (489 genes) versus O (344 genes) identities (as defined by SCDE) in each cell population. A gene is considered as expressed in a given population if its abundance is >1TPM in at least 25% of the cells. NB-identity genes are progressively turned down whereas O-identity genes are progressively activated during the NB to O conversion.

(C) Immunolabeling for neuronal (PSA-NCAM, Tuj1) and oligodendrocyte (Olig2, Cspg4, Pdgfra, Sox10) genes in the SVZ and CC of GAD67-GFP mice 6 days after LPC injection confirm that OligNBL have a dual NB/O identity.

(D) Percentage of Edu^+ cells in NBL (GFP^+), OL ($Tomato^+$), OligNBL (GFP^+, $Tomato^+$) and GFP^- $Tomato^-$ cell populations deriving from the SVZ and CC of GAD67-GFP:Olig2-tdTomato mice 6 days after LPC injection.

Altogether, these results suggested that SVZ NB fate conversion proceeds through formation of an intermediate cell type, the OligNBL, that co-expresses neuronal and oligodendrocyte markers. This intermediate cell type no dot proliferates when characterized 6 days post lesion.

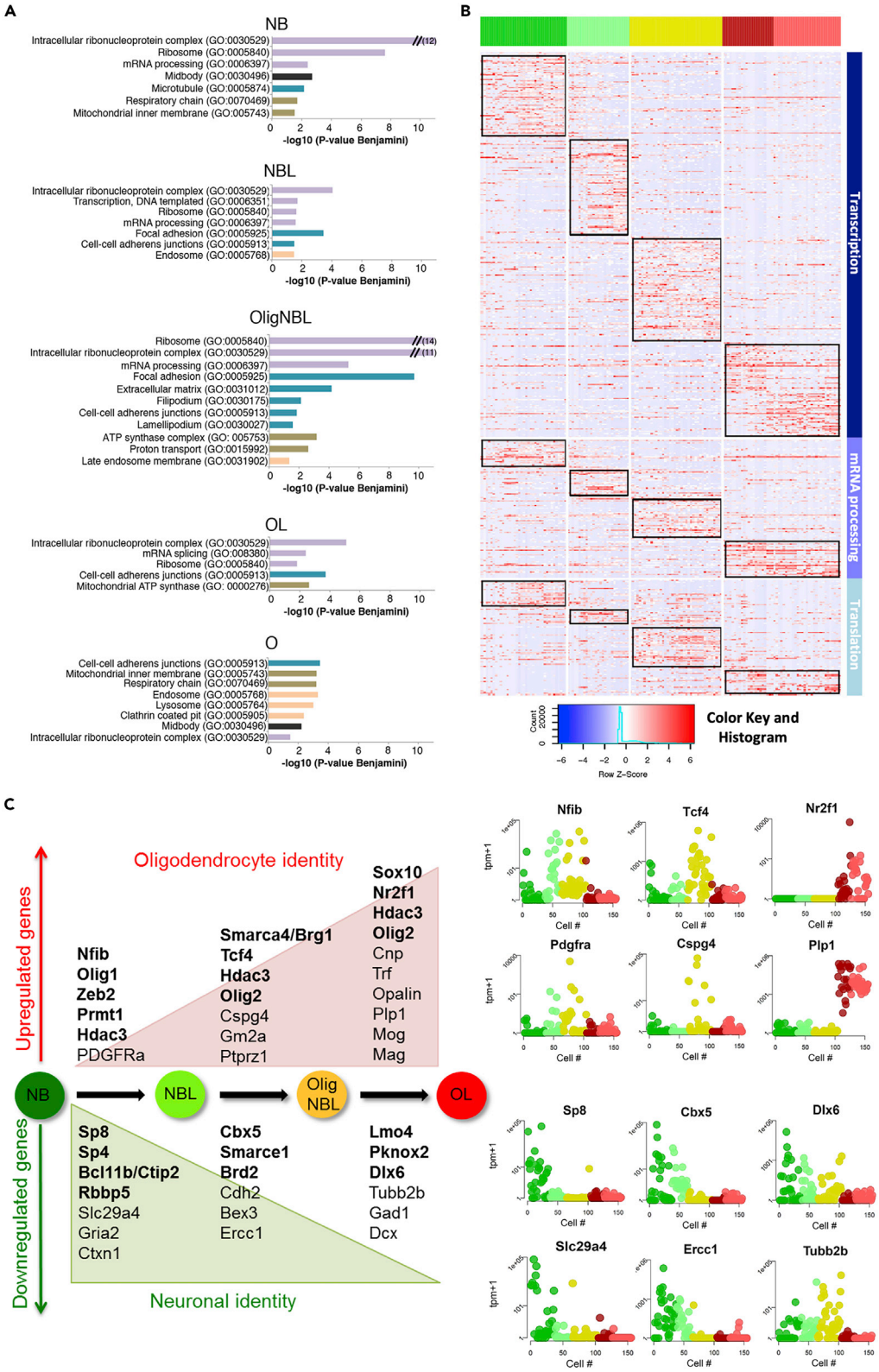
A
NB
Intracellular ribonucleoprotein complex (GO:0030529)
Ribosome (GO:0005840)
mRNA processing (GO:0006397)
Midbody (GO:0030496)
Microtubule (GO:0005874)
Respiratory chain (GO:0070469)
Mitochondrial inner membrane (GO:005743)
-log10 (P-value Benjamini)
NBL
Intracellular ribonucleoprotein complex (GO:0030529)
Transcription, DNA templated (GO:0006351)
Ribosome (GO:0005840)
mRNA processing (GO:0006397)
Focal adhesion (GO:0005925)
Cell-cell adherens junctions (GO:0005913)
Endosome (GO:0005768)
-log10 (P-value Benjamini)
OligNBL
Ribosome (GO:0005840)
Intracellular ribonucleoprotein complex (GO:0030529)
mRNA processing (GO:0006397)
Focal adhesion (GO:0005925)
Extracellular matrix (GO:0031012)
Filipodium (GO:0030175)
Cell-cell adherens junctions (GO:0005913)
Lamellipodium (GO:0030027)
ATP synthase complex (GO: 005753)
Proton transport (GO:0015992)
Late endosome membrane (GO:0031902)
-log10 (P-value Benjamini)
OL
Intracellular ribonucleoprotein complex (GO:0030529)
mRNA splicing (GO:008380)
Ribosome (GO:0005840)
Cell-cell adherens junctions (GO:0005913)
Mitochondrial ATP synthase (GO: 0000276)
-log10 (P-value Benjamini)
O
Cell-cell adherens junctions (GO:0005913)
Mitochondrial inner membrane (GO:0005743)
Respiratory chain (GO:0070469)
Endosome (GO:0005768)
Lysosome (GO:0005764)
Clathrin coated pit (GO:0005905)
Midbody (GO:0030496)
Intracellular ribonucleoprotein complex (GO:0030529)
-log10 (P-value Benjamini)
B
Transcription
mRNA processing
Translation
Color Key and Histogram
Row Z-Score
C
Oligodendrocyte identity
Upregulated genes
Downregulated genes
Neuronal identity
NB
NBL
Olig NBL
OL
Nfib
Olig1
Zeb2
Prmt1
Hdac3
PDGFRa
Smarca4/Brg1
Tcf4
Hdac3
Olig2
Cspg4
Gm2a
Ptprz1
Sox10
Nr2f1
Hdac3
Olig2
Cnp
Trf
Opalin
Plp1
Mog
Mag
Sp8
Sp4
Bcl11b/Ctip2
Rbbp5
Slc29a4
Gria2
Ctxn1
Cbx5
Smarce1
Brd2
Cdh2
Bex3
Ercc1
Lmo4
Pknox2
Dlx6
Tubb2b
Gad1
Dcx
Nfib
Tcf4
Nr2f1
Pdgfra
Cspg4
Plp1
Sp8
Cbx5
Dlx6
Slc29a4
Ercc1
Tubb2b
tpm+1
Cell #

Figure 5. LPC-induced demyelination modifies the transcriptional state of SVZ neuroblasts

(A) GO-term analyses of the 5 cell populations show that their gene-signatures are enriched for functions controlling transcription and translation (purple), cell adhesion and cytoskeleton (blue), cell division (black), respiratory chain (green) and cell trafficking (orange).

(B) Heatmap of mRNA levels for transcription and translation genes in the 5 cell populations. GO terms: transcription (GO: 0,006,351), mRNA processing (GO: 000,639) and ribosome composition (GO: 0,005,840). Red rectangles highlight the set of genes enriched in the gene-signatures of the different populations for each GO-term. A gene is considered as enriched in a cell population if it is differentially expressed between this cell population and at least one other population. Cells are shown in columns and genes in rows.

(C) Summary of characteristic neuronal and oligodendrocyte genes whose expression switches during the various transitions of the fate conversion process. Detailed mRNA levels are given for some oligodendrocyte (Nfib, Tcf4, Nr2f1, PDGFRa, Cspg4, Plp1) and neuronal (Sp8, Cbx5, Dlx6, Slc29a4, Ercc1, Tubb2b) genes.

The key molecular events accompanying NB-to-O fate conversion

To identify the molecular mechanisms driving NB to oligodendrocyte fate conversion, we defined the unique gene-signature of each intermediate state of this fate conversion. To do so, we compared each cell population to the others to find differentially expressed genes within the considered population (using SCDE, Table S8). We found that 586 genes were upregulated in NB as compared to at least one of the other cell populations, 599 genes in NBL, 763 genes in OligNBL, 470 genes in OL and 433 genes in O. To gain insight into the biological function of these genes, we conducted gene ontology (GO) term analyses using DAVID (Figure 5A, Table S9). We found that the five cell population-specific gene-signatures were enriched for functions controlling transcription and translation (purple), cell adhesion and cytoskeleton (blue), cell division (black), respiratory chain (green) and cell trafficking (orange).

We first focused on transcription and translation that were the top enriched biological processes in NB, NBL, OligNBL and OL (Figure 5A). By comparing expression of the genes governing these processes in the 5 cell populations, we found that progression through the intermediate stages of SVZ NB fate conversion involves significant adjustments of the transcription and translation machineries. Indeed, each cell population upregulated expression of distinct gene-sets for controlling transcription (GO: 0,006,351), mRNA processing (GO: 000,639) and ribosome composition (GO: 0,005,840) (Figure 5B and Table S10). To determine how switching from neuronal to oligodendrocyte identities proceeds, we then analyzed expression of the transcriptional regulators known to specify these two identities during the NB/NBL, NBL/OligNBL and OligNBL/OL transitions using SCDE (Figure 5C and Table S11). *(i) NB/NBL transition.* As compared to NB, NBL downregulated expression of transcriptional regulators controlling neuronal development such as the TFs Sp8 (Li et al., 2018), Sp4 (Zhou et al., 2007), Bcl11b/Ctip2 (Simon et al., 2012) and the methyltransferase Rbbp5 (Jiang et al., 2011) Overall, NBL lost expression of half of the genes defining their neuronal identity (269/489 NB-identity genes, Figure 4B and Table S6). Consistent with this loss of neuronal genes, NBL upregulated the histone demethylase KDM5b/JARID1b that negatively regulates neurogenesis (Zhou et al., 2016). Concomitantly, NBL started upregulating transcriptional regulators controlling oligodendrocyte formation and/or differentiation such as the TFs Nfib (Rolando et al., 2016), Olig1 (Lu et al., 2002) and Zeb2 (Weng et al., 2012) as well as the arginine methyltransferase (Hashimoto et al., 2016) and the histone deacetylase Hdac3 that activates Olig2 expression (Zhang et al., 2016). They also upregulated expression of the OPC marker PDGFRa. These results indicate that the identity switch is initiated in NBL, by a partial erasure of the neuronal program concomitant with the onset of activation of genes specifying the oligodendrocyte identity. *(ii) NBL/OligNBL transition.* The intermediate cells OligNBL further repressed their neuronal identity (361/489 NB-identity genes, Figure 4B and Table S6). As compared to NBL, they upregulated the Olig2 target Smarca4/Brg1, a member of the SWI/SNF complex, Hdac3 and the TF Tcf4 which all regulate OPC differentiation and maturation (Figures 5C (Ye et al., 2009)). In addition, OligNBL concomitantly upregulated the OPC markers Cspg4, Ptprz1, Lhfpl3 and Gm2a (Marques et al., 2018). *(iii) OligNBL/OL transition.* OL (Oligodendrocytes after Lesion) originated from two distinct sources: (1) Fate converting OligNBL and (2) pOPC re-activated by the lesion. Sequencing analyses revealed that these two cell populations were highly similar and we therefore treated them as one population (OL). As expected, OL expressed very few genes typically expressed by the neuronal lineage (434/489 NB-identity genes, Figure 4B and Table S6). As compared to OligNBL, they up regulated expression of genes controlling oligodendrocyte maturation such as the transcriptional regulators Sox10, Nr2f1 and Hdac3, as well as mature myelin markers such as Cnp, Trf, Opalin, Plp1, Mog and Mag (Figure 5C). All these results are consistent with our lineage-tracing experiments demonstrating that after demyelinating lesion, SVZ NB start expressing markers of the oligodendrocytes lineage (Olig2,

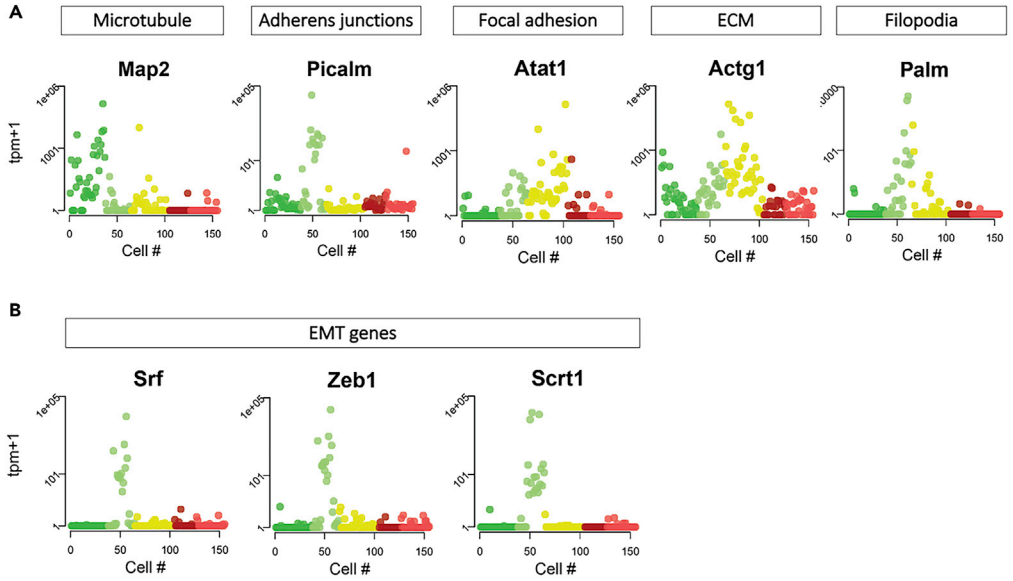

Figure 6. Changes in genes associated with cell migration occurring during SVZ neuroblast fate conversion

(A) Detailed mRNA levels for genes involved in cell adhesion and migration, which are enriched in specific cell populations. Map2 (GO:0,005,874~microtubule) is enriched in NB; Picalm (GO:0,005,913~cell-cell adherens junction) in NBL; Atat1 (GO:0,005,925~focal adhesion) in NBL and OligNBL; Actg1 (GO:0,005,925~focal adhesion and GO:0,031,012~extracellular matrix) in NBL and OligNBL; Palm (GO:0,030,175~filopodium) in OligNBL.

(B) Detailed mRNA levels for genes involved in EMT (Srf, Zeb1, Scrt1), which are specifically upregulated in NBL according to SCDE.

Sox10…) and then convert into fully mature oligodendrocytes expressing MBP and forming functional myelin (see Figure 1).

We next focused on the changes in cell migration. Although acquiring their new identity, SVZ NB switch from a microtubule-dependent chain-like migration to a directed and independent migration toward the lesion (Cayre et al., 2013; Jablonska et al., 2010). We hypothesized that this switch involves a dramatic reorganization of cell-cell contacts and cytoskeletal architecture. Consistent with this, GO term analyses showed that the gene-signature of NB was enriched for genes encoding microtubule proteins, whereas the gene-signature of the intermediate progenitors OligNBL was instead enriched for genes controlling cell adhesion and directed cell migration (Figures 5A and 6A and Table S9). Indeed, OligNBL upregulated expression of focal adhesion and extracellular matrix (ECM) genes, as well as genes controlling lamellipodium and filopodium formation. They also upregulated genes involved in cell guidance such as Slit1, Epha4, Sema3c, Plxna2 and Plxnb2 (Mayor and Etienne-Manneville, 2016) (Table S8). Interestingly, these analyses also revealed that the switch in migration mode is initiated early after lesion induction, in NBL. Indeed, NBL downregulated expression of microtubule genes and their gene signature was enriched for genes controlling cell-cell adherens junction and focal adhesion (Figures 5A and 6A, Table S9). Moreover, differential analyses showed that the NB/NBL transition is characterized by a specific upregulation of a set of TFs controlling epithelial to mesenchymal transition (EMT). As compared to NB, NBL upregulated expression of Zeb1/Zeb2 (Hegarty et al., 2015), Srf (Schwartz et al., 2014) and Scrt1 (Itoh et al., 2013), which have all been shown to control EMT and cell motility (Figure 6B and Table S11). These EMT genes and the N-Cadherin (Cdh2) were down-regulated during the NBL/OligNBL transition, when cells leave the RMS and start their directed migration toward the lesion. Thus, the change from chain-migration to directed-migration is initiated during early stages of the fate conversion process and seems to be controlled by EMT-related mechanisms.

We finally examined the metabolic changes occurring during the intermediate stages of SVZ NB fate conversion. Glycolysis metabolizes glucose into pyruvate, which subsequently enters into the mitochondrial TCA cycle to generate NADH and FADH2 that are in turn used by mitochondrial OXPHOS complexes to produce ATP. The 5 cell populations of the fate conversion process expressed a similar number of genes coding for OXPHOS complexes subunits (Figure 7A). However, the subunit composition of each respiratory

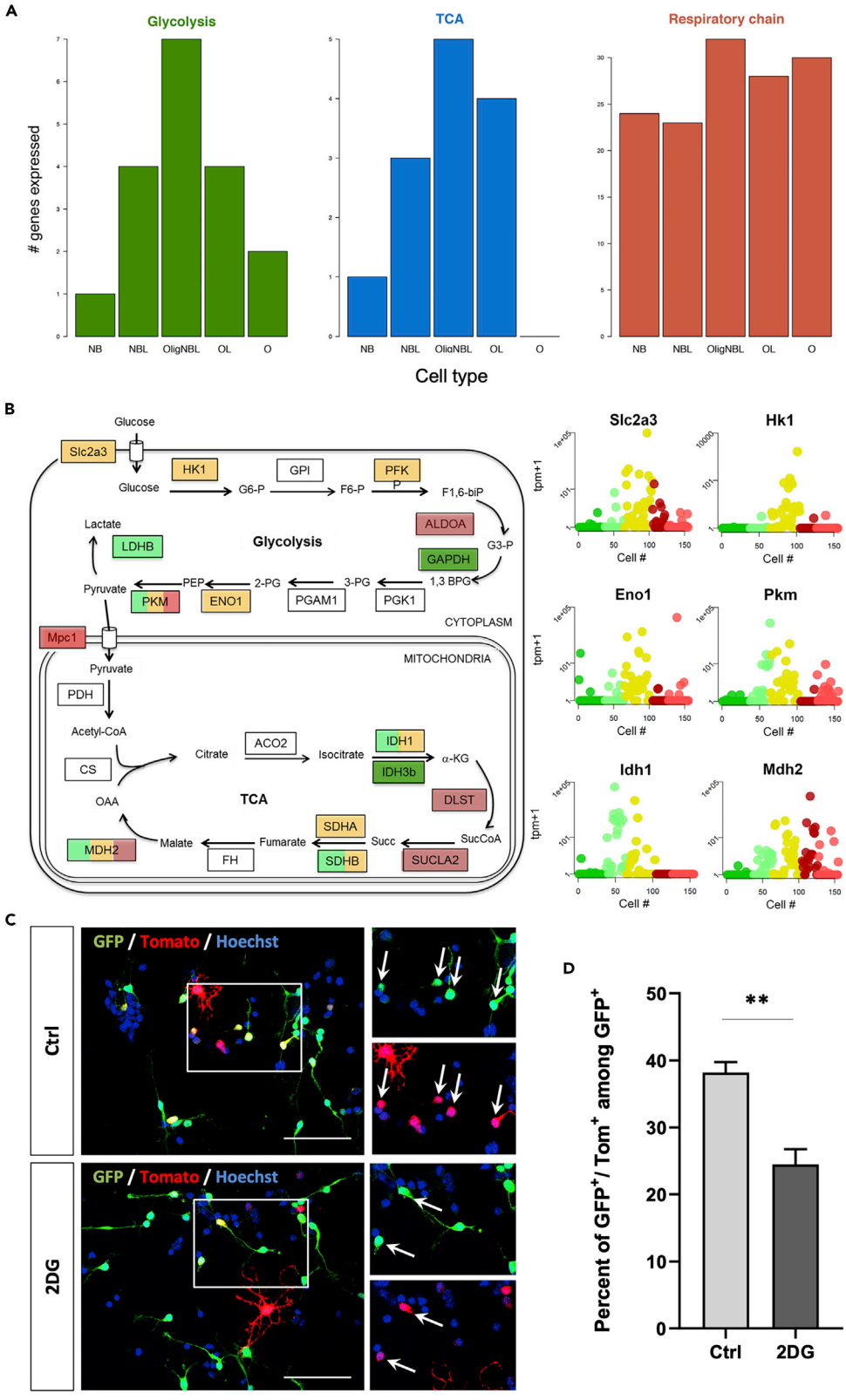
A
Glycolysis
TCA
Respiratory chain
genes expressed
NB
NBL
OligNBL
OL
O
Cell type
B
Glucose
Slc2a3
HK1
GPI
PFK
G6-P
F6-P
F1,6-biP
ALDOA
G3-P
GAPDH
1,3 BPG
PGK1
3-PG
PGAM1
2-PG
ENO1
PEP
PKM
Pyruvate
Lactate
LDHB
Glycolysis
CYTOPLASM
MITOCHONDRIA
Mpc1
Pyruvate
PDH
Acetyl-CoA
CS
Citrate
ACO2
Isocitrate
IDH1
IDH3b
α-KG
DLST
SucCoA
SUCLA2
SDHB
Succ
SDHA
Fumarate
FH
Malate
MDH2
OAA
TCA
Slc2a3
Hk1
Eno1
Pkm
Idh1
Mdh2
tpm+1
Cell #
C
Ctrl
2DG
GFP / Tomato / Hoechst
D
Percent of GFP+/ Tom+ among GFP+
**
Ctrl
2DG

Figure 7. Metabolic changes associated with SVZ NB fate conversion

(A) Number of genes involved in glycolysis (green), TCA cycle (blue) and mitochondrial respiratory chain (red) in each cell population. A gene is considered as expressed in a given population if its abundance is >1TPM in at least 25% of the cells.

(B) Schematic representing the glycolysis pathway and TCA cycle. Genes enriched in specific cell populations are highlighted with the following color-code: green if enriched in NB, light green for NBL, yellow for OligNBL, red for O and dark red for OL. A gene is considered as enriched in a cell population if it is differentially expressed between this cell population and at least one other population. Detailed mRNA levels are given for some glycolysis (Slc2a3, Hk1, Eno1, PKM) and TCA cycle (Idh1, Mdh2) genes.

(C and D) SVZ cells from GAD67-GFP:Olig2-tdTomato neonate mice were cultured in presence or absence of 2DG. GFP^+ $Tomato^+$ cells among GFP^+ cells were observed (C) and quantified (D) in each condition. Scale bars: 50 μm.

complex greatly varied between these populations (Table S13 and Figure S5), thus suggesting that SVZ NB fate conversion does not involve quantitative but instead qualitative changes in OXPHOS. By contrast, we observed a great variation of expression of genes involved in Glycolysis and TCA cycle. As compared to other cell populations, NBL and OligNBL expressed a higher number of glycolysis and TCA genes (Figure 7A and Table S12). Consistent with this, NBL upregulated expression of the glycolytic enzymes PKM and Ldhb as well as the TCA cycle enzymes Idh1, Sdhb and Mdh2 (Figure 7B and Table S13). OligNBL further activated these two pathways by upregulating expression of the glucose transporter Slc2a3, the glycolytic enzymes Hk1, Pfkp, Eno1, and Pkm as well as the TCA cycle enzymes Idh1, Sdha, Sdhb, and Mdh2 (Figure 7B and Table S13). These results strongly suggest that SVZ NB fate conversion requires an increase in glycolytic and TCA pathways activities.

To test this, we investigated the effects of glycolytic inhibition with 2-deoxy-*d*-glucose (2-DG) on NB cell fate conversion, using an *in vitro* assay (Figures 7C and 7D). SVZ derived progenitors from neonate GAD67-GFP:Olig2-tdTomato double transgenic mice were cultured on a Matrigel substrate, which is known to favor their fate conversion. As expected, after 3 days of culture, 38% ± 1.6 of GFP^+ NB were also $Tomato^+$, indicating that they had started their conversion. Interestingly, when NB were cultured with a medium containing 2-DG, the number of GFP^+ $Tomato^+$ cells significantly decreased (Figure 7D), indicating that the fate conversion was less efficient. These results, which are in accordance with our sequencing data, suggest that SVZ NB depend on glycolysis metabolism activity to initiate their fate conversion.

Altogether, these results showed that demyelination signals induce SVZ NBs fate conversion by acting simultaneously on three key processes: (1) They modify/destabilize their transcriptional state to allow co-expression of neuronal and oligodendrocyte genetic programs, (2) they induce their emigration toward demyelinated areas through EMT-related mechanisms, and (3) they change their metabolic status by increasing expression of glycolysis and TCA genes.

DISCUSSION

Spontaneous cell fate conversions are rare events and, as a consequence, the mechanisms controlling these processes *in vivo* remain elusive. In particular, the nature and complexity of the transition states governing these processes are still poorly understood. Spontaneous fate conversions have been documented in the nervous system during development or after injury. These events consistently involve a reversion to an immature state, which can be pluripotent and proliferative. For instance, during *Caenorhabditis elegans* larval stages, rectal cells spontaneously transdifferentiate into neurons. This fate conversion proceeds through discrete steps, without forming a pluripotent state and in the absence of cell division. This conversion goes through a temporary state lacking characteristics of both the initial and final cellular identities (Richard et al., 2011). However, the initial step of this process requires the expression of OSKM genes (Kagias et al., 2012), suggesting that although they do not become pluripotent, these cells revert to an immature state that has a restricted potential. The first example of injury-induced fate conversion was described in the ischemic adult mouse brain (Magnusson et al., 2014). In the striatum of these mice, local astrocytes convert into NB by down-regulating Notch signaling (Magnusson et al., 2014). This fate switch seems to involve a dedifferentiation phase and a proliferative state, because cells transitorily express markers of transient amplifying progenitors (see review (Peron and Berninger, 2015)). More recently, it has been shown that on injury in the mouse olfactory epithelium, some NB acquire multipotency (through an expression of OSKM genes) and proliferate to contribute to olfactory epithelial regeneration by producing both neurons and non-neuronal cells (Lin et al., 2017).

Here, using single cell RNA-sequencing, we show that mice SVZ NB contribute to myelin regeneration by spontaneously converting into oligodendrocytes. This fate conversion occurs without dedifferentiation, by forming

of an intermediate cell type co-expressing markers of the donor (NB) and the target (O) cells. This cell population does not proliferate and does not express OSKM or progenitor cell genes, indicating that it does not revert to an immature state. Of interest, although both cell types emerge from common SVZ progenitor, in physiological condition these two lineages are distinct and this intermediate mixed fate is virtually absent. Therefore, we believe that our work is the first description of a spontaneous cell fate change occurring after brain lesion, which leads to the formation of an intermediate cell type co-expressing two genetic programs.

We demonstrate that this conversion requires tight control of transcriptional and translational activities. It starts in NBL, by the downregulation of key neuronal TFs and chromatin remodelers (e.g., Sp8, Sp4, Bcl11b/Ctip2, and Rbbp5) and the concomitant activation of oligodendrocyte genes (e.g., Olig1, Nfib, Zeb2, and Prmt1). The fate conversion proceeds gradually, by a stepwise downregulation/upregulation of genes controlling the neuronal and oligodendrocyte identities. Thus, the lesion, by dramatically altering the cellular environment, modifies the transcriptional state of SVZ NBs and leads to the formation of a cell type co-expressing two genetic programs. Whether the partial erasure of the neuronal identity of NBL is directly caused by lesional signals or is a consequence of the activation of oligodendrocyte genes remains to be determined.

Our data suggest that a modification of the metabolic status of the cells accompanies SVZ NB fate conversion. We have demonstrated that glycolysis blockage directly impacts NB cell fate conversion. Interestingly, recent studies have shown that the balance between glycolysis and OXPHOS directly impacts cell fate decisions. This has been documented during neuronal differentiation of NSC, cortical neurons maturation and IPSCs differentiation, when cells shift from higher glycolytic metabolism toward an increased OXPHOS state (Gascon et al., 2016). Here, we demonstrate that NB conversion into O involves an increase in glycolysis and TCA cycle activity but not in OXPHOS. Indeed, as compared to NB, NBL and OligNBL express a higher number of glycolytic and TCA cycle genes, in contrast, the number of genes associated with OXPHOS remains stable in all cell populations of the fate conversion continuum. Thus, the progressive loss of the neuronal signature and the concomitant up-regulation of oligodendroglial genes are correlated with an increase in glycolysis and TCA cycle. Of interest, in accordance with our results, down-regulation of glycolytic genes in activated SVZ NSC (compared to quiescent SVZ NSC) correlates with a decrease of expression of glial identity genes and concomitant acquisition of a neuronal fate (Llorens-Bobadilla and Martin-Villalba, 2017). This suggests that an increased glycolytic activity, besides being important for cell fate reprogramming, may be a general feature of oligodendroglial cell identity acquisition (Gascon et al., 2016).

In addition to altering the transcriptional state of a many SVZ NBs, demyelination signals also modify their migratory path by redirecting them toward the areas of damage and cell loss (Cayre et al., 2009; El Waly et al., 2014). Indeed, after lesion, NBs rapidly leave the RMS (Jin et al., 2003) and perform long-distance migration through the brain parenchyma (Cayre et al., 2009). This emigration is facilitated by the growth of blood vessels that form a migration route toward the demyelinated CC (Cayre et al., 2013) and are controlled by numerous factors regulating cell detachment and/or motility (El Waly et al., 2014). Consistent with this, we found that NBL and OligNBL up-regulate expression of genes controlling formation of actin-based protrusive structures such as filopodia and lamellipodia, as well as cell guidance genes. Of interest, our results suggest that EMT-related genes might be involved in SVZ NB emigration. EMT is a biological process allowing polarized epithelial cells to achieve cell fate transformation by enhancing their migratory capacity and increasing their production of extracellular matrix components. Genes from the Zeb and Snail (including Scratch) families are considered master regulators of this process (Lamouille et al., 2014). For instance, Zeb1/2 and Scratch1 have been shown to regulate precursor cell emigration during nervous system development (Ohayon et al., 2016; Itoh et al., 2013; Weng et al., 2012). Of interest, Zeb2, which is positively regulated by Olig1 and Olig2 (Weng et al., 2012), also controls oligodendrocyte maturation (van den Berghe et al., 2013). Our analysis shows that some of these genes are specifically upregulated in NBL. This is notably the case of Zeb1, Zeb2, and Scratch, but also of other factors known to regulate EMT such as Srf and Maz (Luo et al., 2016; Zhao et al., 2016). We therefore propose that EMT related mechanisms participate in cell mobilization after lesion by inducing a loss of cell-cell contacts between chain migrating NBs, thus favoring their emigration outside of the RMS. This is in agreement with the down-regulation of the N-Cadherin (Cdh2) and the up-regulation of the metalloprotease ADAM10 in OligNBL (Table S11), which have both been implicated in the control of SVZ-derived progenitors emigration toward demyelinated lesions (Klingener et al., 2014).

Altogether, our data suggest that in addition to inducing SVZ NB emigration, demyelination signals also destabilize their transcriptional state and modify their metabolic status. The lesion-associated signals

would prime NBs. Of interest, emigration of these 'primed' NB toward the demyelinated CC through EMT-related mechanisms could represent a key step in the fate conversion process, by imposing directionality on the transition and pushing the cells toward the glial fate. In the absence of this emigration, the fate conversion process would then be aborted. Consistent with this hypothesis, we and others have shown that SVZ-derived cells preferentially generate glial cells when grafted in periventricular structures (Cayre et al., 2006) or after lesion-induced mobilization (De Chevigny et al., 2008).

In this study we demonstrate that endogenous NBs from the adult brain display remarkable post-lesion plasticity and can participate to myelin repair through a fate conversion event. Our results indicate that the potential for cell lineage plasticity is present in population of adult brain progenitors after demyelination and that the newly identity is impose by the environment. This study also shows that decision during cell fate identity and differentiation in the adult brain display some plasticity and that a cellular identity can be reached from different origin.

Limitations of the study

In this study, we use a combination of lineage-tracing and single cell RNA-seq to demonstrate that SVZ NB from the mouse adult brain can participate to myelin repair through a fate conversion event. RNA-sequencing has been performed using the GAD67:GFP line, which has been well characterized and specifically labels committed SVZ NB. Lineage-tracing experiments have been done with the DcxCreERT2 line, which is also supposed to be exclusively expressed in SVZ NB. However, because Oligodendrogliogenic and neurogenic adult SVZ neural stem cells constitute distinct lineages, a clonal analysis using DcxCreERT2 line could have help to ultimately demonstrate that a single SVZ NB could generate both oligodendrocyte and neurons after lesion.

STAR★METHODS

Detailed methods are provided in the online version of this paper and include the following:

- KEY RESOURCES TABLE
- RESOURCE AVAILABILITY
  - Lead contact
  - Materials availability
  - Data and code availability
- EXPERIMENTAL MODEL AND SUBJECT DETAILS
  - Transgenic mice
  - SVZ primary cell culture
- METHOD DETAILS
  - Postnatal electroporation
  - Mouse models of demyelination: Lysolecithin and cuprizone
  - EdU labeling
  - Tissue preparation and immunohistochemistry
  - Single-cell preparation and sorting
  - Library preparation and sequencing
- QUANTIFICATION AND STATISTICAL ANALYSIS
  - On mouse brain sections
  - On data analysis
  - Heatmaps were performed using the R function heatmap.2 (package gplots)

SUPPLEMENTAL INFORMATION

Supplemental information can be found online at https://doi.org/10.1016/j.isci.2022.105102.

ACKNOWLEDGMENTS

We are grateful to C. Maurange, B. Prud'homme, X. Caubit, M. Cavey and H. Cremer for critical reading of the manuscript. We thank Bianca Habermann for discussion. This work was funded by CNRS, Aix-Marseille University, the Fondation pour la Recherche Médicale (DEC 20140329501), the ARSEP foundation and the ANR (ANR-21-CE16-0023). We also acknowledge France-bioimaging/PICSL infrastructure (ANR-10-INSB-04-01),

NeuroMarseille institute and NeuroSchool/nEURo*AMU (ANR-17-EURE-0029). BEW was funded by FRM and ARSEP fellowship.

AUTHOR CONTRIBUTIONS

C.B. and B.E.W. conducted, designed the experiments, and wrote the manuscript. M.P. performed bioinformatics analysis and wrote the manuscript. M.F., P.M., and K.M. conducted experiments and commented on the manuscript. M.C. discussed the results and commented on the manuscript. P.D. designed the experiments, supervised the project, and wrote the manuscript.

DECLARATION OF INTERESTS

The authors declare no competing interests.

Received: June 27, 2019
Revised: April 6, 2022
Accepted: September 5, 2022
Published: October 21, 2022

REFERENCES

Berninger, B., Costa, M.R., Koch, U., Schroeder, T., Sutor, B., Grothe, B., and Götz, M. (2007). Functional properties of neurons derived from in vitro reprogrammed postnatal astroglia. J. Neurosci. *27*, 8654–8664. https://doi.org/10.1523/JNEUROSCI.1615-07.2007.

Boutin, C., Diestel, S., Desoeuvre, A., Tiveron, M.C., and Cremer, H. (2008). Efficient in vivo electroporation of the postnatal rodent forebrain. PLoS One *3*, e1883. https://doi.org/10.1371/journal.pone.0001883.

Bray, N.L., Pimentel, H., Melsted, P., and Pachter, L. (2016). Near-optimal probabilistic RNA-seq quantification. Nat. Biotechnol. *34*, 525–527. https://doi.org/10.1038/nbt.3519.

Brousse, B., Magalon, K., Durbec, P., and Cayre, M. (2015). Region and dynamic specificities of adult neural stem cells and oligodendrocyte precursors in myelin regeneration in the mouse brain. Biol. Open *4*, 980–992. https://doi.org/10.1242/bio.012773.

Capilla-Gonzalez, V., Cebrian-Silla, A., Guerrero-Cazares, H., Garcia-Verdugo, J.M., and Quiñones-Hinojosa, A. (2013). The generation of oligodendroglial cells is preserved in the rostral migratory stream during aging. Front. Cell. Neurosci. *7*, 147. https://doi.org/10.3389/fncel.2013.00147.

Cayre, M., Bancila, M., Virard, I., Borges, A., and Durbec, P. (2006). Migrating and myelinating potential of subventricular zone neural progenitor cells in white matter tracts of the adult rodent brain. Mol. Cell. Neurosci. *31*, 748–758. https://doi.org/10.1016/j.mcn.2006.01.004.

Cayre, M., Canoll, P., and Goldman, J.E. (2009). Cell migration in the normal and pathological postnatal mammalian brain. Prog. Neurobiol. *88*, 41–63. https://doi.org/10.1016/j.pneurobio.2009.02.001.

Cayre, M., Courtès, S., Martineau, F., Giordano, M., Arnaud, K., Zamaron, A., and Durbec, P. (2013). Netrin 1 contributes to vascular remodeling in the subventricular zone and promotes progenitor emigration after demyelination. Development *140*, 3107–3117. https://doi.org/10.1242/dev.092999.

Chaker, Z., Codega, P., and Doetsch, F. (2016). Amosaic world: puzzles revealed by adult neural stem cell heterogeneity. Wiley Interdiscip Rev. Dev. Biol. *5*, 640–658. https://doi.org/10.1002/wdev.248.

Chin, M.T. (2014). Reprogramming cell fate: a changing story. Front. Cell Dev. Biol. *2*, 46. https://doi.org/10.3389/fcell.2014.00046.

De Chevigny, A., Cooper, O., Vinuela, A., Reske-Nielsen, C., Lagace, D.C., Eisch, A.J., and Isacson, O. (2008). Fate mapping and lineage analyses demonstrate the production of a large number of striatal neuroblasts after transforming growth factor alpha and noggin striatal infusions into the dopamine-depleted striatum. Stem Cell. *26*, 2349–2360. https://doi.org/10.1634/stemcells.2008-0080.

Decker, L., Picard-Riera, N., Lachapelle, F., and Baron-Van Evercooren, A. (2002). Growth factor treatment promotes mobilization of young but not aged adult subventricular zone precursors in response to demyelination. J. Neurosci. Res. *69*, 763–771. https://doi.org/10.1002/jnr.10411.

Dillies, M.A., Rau, A., Aubert, J., Hennequet-Antier, C., Jeanmougin, M., Servant, N., Keime, C., Marot, G., Castel, D., Estelle, J., et al. (2013). A comprehensive evaluation of normalization methods for Illumina high-throughput RNA sequencing data analysis. Brief. Bioinform. *14*, 671–683. https://doi.org/10.1093/bib/bbs046.

Dulken, B.W., Leeman, D.S., Boutet, S.C., Hebestreit, K., and Brunet, A. (2017). Single-cell transcriptomic analysis Defines Heterogeneity and transcriptional Dynamics in the adult neural stem cell lineage. Cell Rep. *18*, 777–790. https://doi.org/10.1016/j.celrep.2016.12.060.

El Waly, B., Cayre, M., and Durbec, P. (2018). Promoting myelin repair through in vivo neuroblast reprogramming. Stem Cell Rep. *10*, 1492–1504. https://doi.org/10.1016/j.stemcr.2018.02.015.

El Waly, B., Macchi, M., Cayre, M., and Durbec, P. (2014). Oligodendrogenesis in the normal and pathological central nervous system. Front. Neurosci. *8*, 145. https://doi.org/10.3389/fnins.2014.00145.

Gadye, L., Das, D., Sanchez, M.A., Street, K., Baudhuin, A., Wagner, A., Cole, M.B., Choi, Y.G., Yosef, N., Purdom, E., et al. (2017). Injury activates transient olfactory stem cell states with Diverse lineage Capacities. Cell Stem Cell *21*, 775–790.e9. https://doi.org/10.1016/j.stem.2017.10.014.

Gascón, S., Masserdotti, G., Russo, G.L., and Götz, M. (2017). Direct neuronal reprogramming: Achievements, Hurdles, and new Roads to success. Cell Stem Cell *21*, 18–34. https://doi.org/10.1016/j.stem.2017.06.011.

Gascón, S., Murenu, E., Masserdotti, G., Ortega, F., Russo, G.L., Petrik, D., Deshpande, A., Heinrich, C., Karow, M., Robertson, S.P., et al. (2016). Identification and successful Negotiation of a metabolic Checkpoint in direct neuronal reprogramming. Cell Stem Cell *18*, 396–409. https://doi.org/10.1016/j.stem.2015.12.003.

Halley-Stott, R.P., Jullien, J., Pasque, V., and Gurdon, J. (2014). Mitosis gives a brief window of opportunity for a change in gene transcription. PLoS Biol. *12*, e1001914. https://doi.org/10.1371/journal.pbio.1001914.

Hashimoto, M., Murata, K., Ishida, J., Kanou, A., Kasuya, Y., and Fukamizu, A. (2016). Severe Hypomyelination and developmental Defects are caused in mice lacking protein arginine methyltransferase 1 (PRMT1) in the central nervous system. J. Biol. Chem. *291*, 2237–2245. https://doi.org/10.1074/jbc.M115.684514.

Hegarty, S.V., Sullivan, A.M., and O'Keeffe, G.W. (2015). Zeb2: a multifunctional regulator of nervous system development. Prog. Neurobiol. *132*, 81–95. https://doi.org/10.1016/j.pneurobio.2015.07.001.

Heinrich, C., Blum, R., Gascón, S., Masserdotti, G., Tripathi, P., Sánchez, R., Tiedt, S., Schroeder, T., Götz, M., and Berninger, B. (2010). Directing astroglia from the cerebral cortex into subtype specific functional neurons. PLoS Biol. *8*, e1000373. https://doi.org/10.1371/journal.pbio.1000373.

Heins, N., Malatesta, P., Cecconi, F., Nakafuku, M., Tucker, K.L., Hack, M.A., Chapouton, P., Barde, Y.A., and Götz, M. (2002). Glial cells

generate neurons: the role of the transcription factor Pax6. Nat. Neurosci. *5*, 308–315. https://doi.org/10.1038/nn828.

Itoh, Y., Moriyama, Y., Hasegawa, T., Endo, T.A., Toyoda, T., and Gotoh, Y. (2013). Scratch regulates neuronal migration onset via an epithelial-mesenchymal transition-like mechanism. Nat. Neurosci. *16*, 416–425. https://doi.org/10.1038/nn.3336.

Jablonska, B., Aguirre, A., Raymond, M., Szabo, G., Kitabatake, Y., Sailor, K.A., Ming, G.L., Song, H., and Gallo, V. (2010). Chordin-induced lineage plasticity of adult SVZ neuroblasts after demyelination. Nat. Neurosci. *13*, 541–550. https://doi.org/10.1038/nn.2536.

Jessen, K.R., Mirsky, R., and Arthur-Farraj, P. (2015). The role of cell plasticity in tissue repair: Adaptive cellular reprogramming. Dev. Cell *34*, 613–620. https://doi.org/10.1016/j.devcel.2015.09.005.

Jiang, H., Shukla, A., Wang, X., Chen, W.Y., Bernstein, B.E., and Roeder, R.G. (2011). Role for Dpy-30 in ES cell-fate specification by regulation of H3K4 methylation within bivalent domains. Cell *144*, 513–525. https://doi.org/10.1016/j.cell.2011.01.020.

Jin, K., Sun, Y., Xie, L., Peel, A., Mao, X.O., Batteur, S., and Greenberg, D.A. (2003). Directed migration of neuronal precursors into the ischemic cerebral cortex and striatum. Mol. Cell. Neurosci. *24*, 171–189. https://doi.org/10.1016/s1044-7431(03)00159-3.

Jopling, C., Boue, S., and Izpisua Belmonte, J.C. (2011). Dedifferentiation, transdifferentiation and reprogramming: three routes to regeneration. Nat. Rev. Mol. Cell Biol. *12*, 79–89.

Kagias, K., Ahier, A., Fischer, N., and Jarriault, S. (2012). Members of the NODE (Nanog and Oct4-associated deacetylase) complex and SOX-2 promote the initiation of a natural cellular reprogramming event in vivo. Proc. Natl. Acad. Sci. USA *109*, 6596–6601. https://doi.org/10.1073/pnas.1117031109.

Kharchenko, P.V., Silberstein, L., and Scadden, D.T. (2014). Bayesian approach to single-cell differential expression analysis. Nat. Methods *11*, 740–742. https://doi.org/10.1038/nmeth.2967.

Klein, B., Mrowetz, H., Kreutzer, C., Rotheneichner, P., Zaunmair, P., Lange, S., Coras, R., Couillard-Despres, S., Rivera, F.J., and Aigner, L. (2020). DCX(+) neuronal progenitors contribute to new oligodendrocytes during remyelination in the hippocampus. Sci. Rep. *10*, 20095. https://doi.org/10.1038/s41598-020-77115-w.

Klingener, M., Chavali, M., Singh, J., McMillan, N., Coomes, A., Dempsey, P.J., Chen, E.I., and Aguirre, A. (2014). N-cadherin promotes recruitment and migration of neural progenitor cells from the SVZ neural stem cell niche into demyelinated lesions. J. Neurosci. *34*, 9590–9606. https://doi.org/10.1523/JNEUROSCI.3699-13.2014.

Lamouille, S., Xu, J., and Derynck, R. (2014). Molecular mechanisms of epithelial-mesenchymal transition. Nat. Rev. Mol. Cell Biol. *15*, 178–196. https://doi.org/10.1038/nrm3758.

Li, J., Wang, C., Zhang, Z., Wen, Y., An, L., Liang, Q., Xu, Z., Wei, S., Li, W., Guo, T., et al. (2018). Transcription factors Sp8 and Sp9 coordinately regulate olfactory bulb Interneuron development. Cereb. Cortex *28*, 3278–3294. https://doi.org/10.1093/cercor/bhx199.

Lin, B., Coleman, J.H., Peterson, J.N., Zunitch, M.J., Jang, W., Herrick, D.B., and Schwob, J.E. (2017). Injury induces endogenous reprogramming and dedifferentiation of neuronal progenitors to multipotency. Cell Stem Cell *21*, 761–774.e5. https://doi.org/10.1016/j.stem.2017.09.008.

Llorens-Bobadilla, E., and Martin-Villalba, A. (2017). Adult NSC diversity and plasticity: the role of the niche. Curr. Opin. Neurobiol. *42*, 68–74. https://doi.org/10.1016/j.conb.2016.11.008.

Lois, C., and Alvarez-Buylla, A. (1994). Long-distance neuronal migration in the adult mammalian brain. Science *264*, 1145–1148. https://doi.org/10.1126/science.8178174.

Lois, C., García-Verdugo, J.M., and Alvarez-Buylla, A. (1996). Chain migration of neuronal precursors. Science *271*, 978–981. https://doi.org/10.1126/science.271.5251.978.

Lu, Q.R., Sun, T., Zhu, Z., Ma, N., Garcia, M., Stiles, C.D., and Rowitch, D.H. (2002). Common developmental requirement for Olig function indicates a motor neuron/oligodendrocyte connection. Cell *109*, 75–86. https://doi.org/10.1016/s0092-8674(02)00678-5.

Luo, W., Zhu, X., Liu, W., Ren, Y., Bei, C., Qin, L., Miao, X., Tang, F., Tang, G., and Tan, S. (2016). MYC associated zinc finger protein promotes the invasion and metastasis of hepatocellular carcinoma by inducing epithelial mesenchymal transition. Oncotarget *7*, 86420–86432. https://doi.org/10.18632/oncotarget.13416.

Magnusson, J.P., Göritz, C., Tatarishvili, J., Dias, D.O., Smith, E.M.K., Lindvall, O., Kokaia, Z., and Frisén, J. (2014). A latent neurogenic program in astrocytes regulated by Notch signaling in the mouse. Science *346*, 237–241. https://doi.org/10.1126/science.346.6206.237.

Marques, S., van Bruggen, D., Vanichkina, D.P., Floriddia, E.M., Munguba, H., Väremo, L., Giacomello, S., Falcão, A.M., Meijer, M., Björklund, Å.K., et al. (2018). Transcriptional Convergence of oligodendrocyte lineage progenitors during development. Dev. Cell *46*, 504–517.e7. https://doi.org/10.1016/j.devcel.2018.07.005.

Mayor, R., and Etienne-Manneville, S. (2016). The front and rear of collective cell migration. Nat. Rev. Mol. Cell Biol. *17*, 97–109. https://doi.org/10.1038/nrm.2015.14.

McKay, N.D., Robinson, B., Brodie, R., and Rooke-Allen, N. (1983). Glucose transport and metabolism in cultured human skin fibroblasts. Biochim. Biophys. Acta *762*, 198–204. https://doi.org/10.1016/0167-4889(83)90071-x.

Menn, B., Garcia-Verdugo, J.M., Yaschine, C., Gonzalez-Perez, O., Rowitch, D., and Alvarez-Buylla, A. (2006). Origin of oligodendrocytes in the subventricular zone of the adult brain. J. Neurosci. *26*, 7907–7918. https://doi.org/10.1523/JNEUROSCI.1299-06.2006.

Moris, N., Pina, C., and Arias, A.M. (2016). Transition states and cell fate decisions in epigenetic landscapes. Nat. Rev. Genet. *17*, 693–703. https://doi.org/10.1038/nrg.2016.98.

Muzumdar, M.D., Tasic, B., Miyamichi, K., Li, L., and Luo, L. (2007). A global double-fluorescent Cre reporter mouse. Genesis *45*, 593–605. https://doi.org/10.1002/dvg.20335.

Ohayon, D., Garcès, A., Joly, W., Soukkarieh, C., Takagi, T., Sabourin, J.C., Agius, E., Darling, D.S., De Santa Barbara, P., Higashi, Y., et al. (2016). Onset of Spinal Cord astrocyte precursor emigration from the ventricular zone involves the Zeb1 transcription factor. Cell Rep. *17*, 1473–1481. https://doi.org/10.1016/j.celrep.2016.10.016.

Péron, S., and Berninger, B. (2015). Reawakening the sleeping beauty in the adult brain: neurogenesis from parenchymal glia. Curr. Opin. Genet. Dev. *34*, 46–53. https://doi.org/10.1016/j.gde.2015.07.004.

Picelli, S., Faridani, O.R., Björklund, A.K., Winberg, G., Sagasser, S., and Sandberg, R. (2014). Full-length RNA-seq from single cells using Smart-seq2. Nat. Protoc. *9*, 171–181. https://doi.org/10.1038/nprot.2014.006.

Qiu, X., Mao, Q., Tang, Y., Wang, L., Chawla, R., Pliner, H.A., and Trapnell, C. (2017). Reversed graph embedding resolves complex single-cell trajectories. Nat. Methods *14*, 979–982. https://doi.org/10.1038/nmeth.4402.

R Core Team (2017). R: a language and environment for statistical computing. In R Foundation for Statistical Computing (R Core Team).

Richard, J.P., Zuryn, S., Fischer, N., Pavet, V., Vaucamps, N., and Jarriault, S. (2011). Direct in vivo cellular reprogramming involves transition through discrete, non-pluripotent steps. Development *138*, 1483–1492. https://doi.org/10.1242/dev.063115.

Rivers, L.E., Young, K.M., Rizzi, M., Jamen, F., Psachoulia, K., Wade, A., Kessaris, N., and Richardson, W.D. (2008). PDGFRA/NG2 glia generate myelinating oligodendrocytes and piriform projection neurons in adult mice. Nat. Neurosci. *11*, 1392–1401. https://doi.org/10.1038/nn.2220.

Rolando, C., Erni, A., Grison, A., Beattie, R., Engler, A., Gokhale, P.J., Milo, M., Wegleiter, T., Jessberger, S., and Taylor, V. (2016). Multipotency of adult hippocampal NSCs in vivo is restricted by Drosha/NFIB. Cell Stem Cell *19*, 653–662. https://doi.org/10.1016/j.stem.2016.07.003.

Ruiz, S., Panopoulos, A.D., Herrerías, A., Bissig, K.D., Lutz, M., Berggren, W.T., Verma, I.M., and Izpisua Belmonte, J.C. (2011). A high proliferation rate is required for cell reprogramming and maintenance of human embryonic stem cell identity. Curr. Biol. *21*, 45–52. https://doi.org/10.1016/j.cub.2010.11.049.

Schneider, C.A., Rasband, W.S., and Eliceiri, K.W. (2012). NIH Image to ImageJ: 25 years of image analysis. Nat. Methods *9*, 671–675. https://doi.org/10.1038/nmeth.2089.

Schwartz, B., Marks, M., Wittler, L., Werber, M., Währisch, S., Nordheim, A., Herrmann, B.G., and Grote, P. (2014). SRF is essential for mesodermal

cell migration during elongation of the embryonic body axis. Mech. Dev. *133*, 23–35. https://doi.org/10.1016/j.mod.2014.07.001.

Sieweke, M.H. (2015). Waddington's valleys and Captain Cook's islands. Cell Stem Cell *16*, 7–8. https://doi.org/10.1016/j.stem.2014.12.009.

Simon, R., Brylka, H., Schwegler, H., Venkataramanappa, S., Andratschke, J., Wiegreffe, C., Liu, P., Fuchs, E., Jenkins, N.A., Copeland, N.G., et al. (2012). A dual function of Bcl11b/Ctip2 in hippocampal neurogenesis. The EMBO journal *31*, 2922–2936. https://doi.org/10.1038/emboj.2012.142.

Srinivas, S., Watanabe, T., Lin, C.S., William, C.M., Tanabe, Y., Jessell, T.M., and Costantini, F. (2001). Cre reporter strains produced by targeted insertion of EYFP and ECFP into the ROSA26 locus. BMC Dev. Biol. *1*, 4. https://doi.org/10.1186/1471-213x-1-4.

Takahashi, K., and Yamanaka, S. (2016). A decade of transcription factor-mediated reprogramming to pluripotency. Nat. Rev. Mol. Cell Biol. *17*, 183–193. https://doi.org/10.1038/nrm.2016.8.

Tamamaki, N., Yanagawa, Y., Tomioka, R., Miyazaki, J.I., Obata, K., and Kaneko, T. (2003). Green fluorescent protein expression and colocalization with calretinin, parvalbumin, and somatostatin in the GAD67-GFP knock-in mouse. J. Comp. Neurol. *467*, 60–79. https://doi.org/10.1002/cne.10905.

Tata, P.R., and Rajagopal, J. (2016). Cellular plasticity: 1712 to the present day. Curr. Opin. Cell Biol. *43*, 46–54. https://doi.org/10.1016/j.ceb.2016.07.005.

Tsacopoulos, M., and Magistretti, P.J. (1996). Metabolic coupling between glia and neurons. J. Neurosci. *16*, 877–885. https://doi.org/10.1523/JNEUROSCI.16-03-00877.1996.

van den Berghe, V., Stappers, E., Vandesande, B., Dimidschstein, J., Kroes, R., Francis, A., Conidi, A., Lesage, F., Dries, R., Cazzola, S., et al. (2013). Directed migration of cortical interneurons depends on the cell-autonomous action of Sip1. Neuron *77*, 70–82. https://doi.org/10.1016/j.neuron.2012.11.009.

Waddington, C.H. (1968). Towards a theoretical biology. Nature *218*, 525–527. https://doi.org/10.1038/218525a0.

Weng, Q., Chen, Y., Wang, H., Xu, X., Yang, B., He, Q., Shou, W., Chen, Y., Higashi, Y., van den Berghe, V., et al. (2012). Dual-mode modulation of Smad signaling by Smad-interacting protein Sip1 is required for myelination in the central nervous system. Neuron *73*, 713–728. https://doi.org/10.1016/j.neuron.2011.12.021.

Weng, Q., Wang, J., Wang, J., He, D., Cheng, Z., Zhang, F., Verma, R., Xu, L., Dong, X., Liao, Y., et al. (2019). Single-cell transcriptomics Uncovers glial progenitor diversity and cell fate Determinants during development and Gliomagenesis. Cell Stem Cell *24*, 707–723.e8. https://doi.org/10.1016/j.stem.2019.03.006.

Wichterle, H., Garcia-Verdugo, J.M., and Alvarez-Buylla, A. (1997). Direct evidence for homotypic, glia-independent neuronal migration. Neuron *18*, 779–791. https://doi.org/10.1016/s0896-6273(00)80317-7.

Xing, Y.L., Röth, P.T., Stratton, J.A.S., Chuang, B.H.A., Danne, J., Ellis, S.L., Ng, S.W., Kilpatrick, T.J., and Merson, T.D. (2014). Adult neural precursor cells from the subventricular zone contribute significantly to oligodendrocyte regeneration and remyelination. J. Neurosci. *34*, 14128–14146. https://doi.org/10.1523/JNEUROSCI.3491-13.2014.

Ye, F., Chen, Y., Hoang, T., Montgomery, R.L., Zhao, X.H., Bu, H., Hu, T., Taketo, M.M., van Es, J.H., Clevers, H., et al. (2009). HDAC1 and HDAC2 regulate oligodendrocyte differentiation by disrupting the beta-catenin-TCF interaction. Nat. Neurosci. *12*, 829–838. https://doi.org/10.1038/nn.2333.

Zeisel, A., Muñoz-Manchado, A.B., Codeluppi, S., Lönnerberg, P., La Manno, G., Juréus, A., Marques, S., Munguba, H., He, L., Betsholtz, C., et al. (2015). Brain structure. Cell types in the mouse cortex and hippocampus revealed by single-cell RNA-seq. Science *347*, 1138–1142. https://doi.org/10.1126/science.aaa1934.

Zhang, J., Nuebel, E., Daley, G.Q., Koehler, C.M., and Teitell, M.A. (2012). Metabolic regulation in pluripotent stem cells during reprogramming and self-renewal. Cell Stem Cell *11*, 589–595. https://doi.org/10.1016/j.stem.2012.10.005.

Zhang, L., He, X., Liu, L., Jiang, M., Zhao, C., Wang, H., He, D., Zheng, T., Zhou, X., Hassan, A., et al. (2016). Hdac3 interaction with p300 histone Acetyltransferase regulates the oligodendrocyte and astrocyte lineage fate switch. Dev. Cell *37*, 582. https://doi.org/10.1016/j.devcel.2016.06.004.

Zhao, L., Zhao, J., Wang, X., Chen, Z., Peng, K., Lu, X., Meng, L., Liu, G., Guan, G., and Wang, F. (2016). Serum response factor induces endothelial-mesenchymal transition in glomerular endothelial cells to aggravate proteinuria in diabetic nephropathy. Physiol. Genomics *48*, 711–718. https://doi.org/10.1152/physiolgenomics.00082.2016.

Zhou, Q., Obana, E.A., Radomski, K.L., Sukumar, G., Wynder, C., Dalgard, C.L., and Doughty, M.L. (2016). Inhibition of the histone demethylase Kdm5b promotes neurogenesis and derepresses Reln (reelin) in neural stem cells from the adult subventricular zone of mice. Mol. Biol. Cell *27*, 627–639. https://doi.org/10.1152/physiolgenomics.00082.2016.

Zhou, X., Qyang, Y., Kelsoe, J.R., Masliah, E., and Geyer, M.A. (2007). Impaired postnatal development of hippocampal dentate gyrus in Sp4 null mutant mice. Genes Brain Behav. *6*, 269–276. https://doi.org/10.1111/j.1601-183X.2006.00256.x.

STAR★METHODS

KEY RESOURCES TABLE

REAGENT or RESOURCE	SOURCE	IDENTIFIER
Antibodies		
Chicken polyclonal anti-GFP	Aves Labs	Cat#GFP-1020; RRID:AB_10000240
Mouse monoclonal anti-beta III Tubulin	Eurogentec	Cat#MMS-435P-100 ; RRID: AB_2313773
Mouse monoclonal anti-MBP	Chemicon	Cat#MAB384; RRID:AB_240837
Rabbit polyclonal anti-Olig-2	Chemicon	Cat#AB9610; RRID:AB_570666
Rat monoclonal anti-Pdgfra	Chemicon	Cat#CBL1366; RRID:AB_2283679
Rat monoclonal anti-Sox10	Santa Cruz	Cat#sc-17342; RRID:AB_2195374
Mouse monoclonal Anti PSA-NCAM	ThermoFisher	Cat# 14-9118-82
Mouse monoclonal anti Csp4/NG2	Chemicon	Cat#MAB5384; RRID:AB_177646
Biological samples		
Sub-ventricular zone and Corpus callosum (Brains)	Transgenic mice	N/A
Chemicals, peptides, and recombinant proteins		
Neural tissue dissociation kit	Miltenyi Biotec	Cat#130-092-628
Fixable Viability Dye eFluor780	Thermofisher	Cat#65-0865-14
Illumina Nextera XT sample preparation	Illumina	Cat#FC-131-1002
Deposited data		
All reads of the Single Cell RNA Sequencing	NCBI GEO	GSE130355
Experimental models: Organisms/strains		
Heterozygous GAD67-GFP transgenic mice	Tamamaki et al., 2003	
Mouse Olig2-tdTomato TH39Gsat/Mmcd	MMRRC	036530-UCD
Gad67-GFP:Olig2-tdTomato mice	Our Lab	N/A
Homozygous R26R-YFP	Srinivas et al., 2001	N/A
Neonate homozygous mT/mG mice	Muzumdar et al., 2007	N/A
Tg(DCX-cre/ERT2)1Mull mouse line	The Jackson laboratory	MGI: 5014069
DCX-CreERT2 mice crossed to R26R-YFP or mTmG	Our Lab	N/A
Software and algorithms		
Fiji	Schneider et al., 2012	RRID: SCR_002285
Zen software 2012	ZEISS	Zen Black RRID:SCR_018163
normalizeBetweenArrays	R package limma	N/A
Heatmaps	R function heatmap.2	package gplots
PCA analyses / dudi.pca	R package ade4	v1.7.11
two-way unsupervised clustering approach	Zeisel et al., 2015	BACKSPIN v3.5
Pseudo-temporal ordering	R package monocle	v2.6.4
Differential expression analysis	R package SCDE	v2.6.0
GO-term analyses	DAVID 6.8	RRID:SCR_001881

RESOURCE AVAILABILITY

Lead contact

Further information and requests for reagents may be directed to, and will be fulfilled by the corresponding author, Dr. Pascale Durbec (Pascale.durbec@univ-amu.fr).

Materials availability

This study did not generate new unique reagents. RNA-seq data have been deposited into suitable repositories.

Data and code availability

- Single-cell RNA-seq data have been deposited at GEO and are publicly available as of the date of publication. Accession numbers are listed in the key resources table.
- This article does not report original code.
- All other items: Any additional information required to reanalyze the data reported in this article is available from the lead contact on request.

EXPERIMENTAL MODEL AND SUBJECT DETAILS

Transgenic mice

All breeding, experimental and surgical protocols were performed following the guidelines established by the French Ministry of Agriculture (Animal Rights Division). The architecture and functioning rules of our animal house, as well as our experimental procedures have been approved by the "Direction Départementale des Services Vétérinaires" and the ethic committee (ID numbers F1305521 and 2016071112151400 for animal house and research project, respectively).

Heterozygous male and female GAD67-GFP transgenic mice (8-10 weeks old) (Tamamaki et al., 2003) were used to label neuroblasts. Adult male and female Olig2-tdTomato TH39Gsat/Mmcd (Mutant Mouse Regional Resource Center Figure S3) were used to label OLG cell lineage. Detailed characterization of the Olig2-tdTomato mouse line is presented in Figure S3. In brief, these analyses showed that in the CC and cortex of 8 weeks old mice, 80% of Olig2+ cells expressed Tomato. Conversely, around 70% of Tomato + cells also expressed Olig2. These mice were crossed to generate GAD67-GFP:Olig2-tdTomato double transgenic mice in which neuroblasts and oligodendrocyte lineage cells are labeled in green and red, respectively. GAD67-GFP:Olig2-tdTomato mice (8–10 weeks old males and females were then used to purify NB, NBL, OligNBL, O and OL for subsequent single cell RNA-sequencing experiments. Neonate homozygous mT/mG mice (Muzumdar et al., 2007) were used to lineage-trace SVZ neuroblasts after cuprizone-induced demyelination. Homozygous R26R-YFP (Srinivas et al., 2001) reporters were used to generate double-heterozygous offspring by crossing with DCX-CreERT2 (Tg(DCX-cre/ERT2) 1Mull mouse line from the Jackson). To perform long term tracing of NB, adult DCX-CreERT2 mice crossed to R26R-YFP or mTmG and were fed 5 consecutive days with tamoxifen (180 mg/kg). Tracing in mTmG mice was performed using electroporation. Neonate homozygous mTmG mice were electroporated with a pDCX-CreERT2 plasmid (El Waly et al., 2018). Five weeks after electroporation, cuprizone treatment started, and one more week later these mice were injected for 5 consecutive days with tamoxifen (180 mg/kg) to induce recombination and NBL labeling. For all experiments, we worked to ensure sex balance in the selection of mouse and used equivalent number of male and female subjects in the various cohorts to ensure reduction if number of generated mice and because no influence of sex on the mechanisms studied has been reported.

The transcriptome of mouse brain cells was performed in the laboratory of Dr. Pascale Durbec. 155 cells undergoing reprogramming were collected after focal demyelination in the corpus callosum of adult mice. Mice, stereotactic surgeries and samples were handled according to French laws and regulations, with the approval of the "Direction Départementale des Services Vétérinaires" and the ethic committee (ID numbers F1305521 and 2,016,071,112,151,400 for animal house and research project, respectively).

SVZ primary cell culture

Brains of 3-day-old GAD67-GFP:Olig2-tdTomato mice were dissected out and sectioned into 400 μm thick slices using a vibratome (Leica Microsystems, Rueil-Malmaison, France). SVZ was dissected in Hank's Balanced Salt Solution. Dissociated cells were cultured in serum-free medium containing B-27 supplement.

(Life Technologies) on a Matrigel coating (33%) in presence or absence of 2mM 2-DG in the medium. Cells were analyzed after fixation 3 days after plating.

METHOD DETAILS

Postnatal electroporation

Electroporation of postnatal animals was performed as previously described in Boutin et al. (2008) as follow: Pups were anesthetized by hypothermia and 2 μL of endotoxin-free plasmids (3 μg/μL) were injected into the left lateral ventricle. After injection, pups were subjected to five 95 V electrical pulses (50 ms, separated by 950 ms intervals) using the CUY21 edit device (Nepa Gene).

Mouse models of demyelination: Lysolecithin and cuprizone

Lysolecithin (LPC)-induced focal demyelination was performed as originally described by Decker et al., (2002) with minor modifications. Briefly, 8–10 weeks old (male and female) GAD67-GFP:Olig2-td. Tomato mice were anesthetized and placed in a stereotactic frame (Kopf). 0.7 μL of a solution of 1% LPC (Sigma) in 0.9% NaCl was injected unilaterally into the CC (1.5 mm anterior, 1 mm lateral to bregma, 2 mm deep from cortical surface). Cuprizone treatment (0.2% in food) was given for 5 weeks either to 8–10 weeks old GAD67-GFP mice or to mTmG mice 5 weeks after electroporation.

EdU labeling

Two hours before sacrifice, animals received one Intra-peritoneal injection of EdU (100 mg/kg in PBS). EdU staining was performed on 50 μM sections using Click-iTTM EdU protocol (Invitrogen, Carlsbad, CA). Briefly, sections were incubated with a Click-iT™ reaction cocktail containing Click-iT™ reaction buffer, CuSO4, Alexa Fluor® 647, and reaction buffer additive for 30 min, then rinsed, DAPI counterstained and mounted.

Tissue preparation and immunohistochemistry

Mice were transcardially perfused with 4% paraformaldehyde. The brains were removed, post-fixed overnight and cut into 50 μm coronal or sagittal sections using a vibratome (Leica Microsystem, Rueil Malmaison, France). Immunofluorescent labeling was performed on sections. The following antibodies were used: anti-GFP (chicken, 1/500, Aves Labs), anti-BIII tubulin (Tuj-1, mouse IgG2, 1/100), anti-MBP (mouse IgG1, 1/500, Chemicon), anti-Olig2 (rabbit, 1/500, Chemicon), anti-Pdgfra (rat IgG2, 1/250, Chemicon), anti-Sox10 (goat, 1/200, Santa Cruz), anti PSA-NCAM (MenB, 1/2, mouse IgM from our laboratory), anti Csp4/NG2 (mouse IgG1, 1/200, Chemicon). The sections were incubated with appropriate Alexa-conjugated secondary antibodies (1/500, Jackson ImmunoResearch Laboratories) then counterstained with Hoechst 33342 (1/500, Sigma). Images were captured with a Zeiss ApoTome system (20× and 60× objectives) and a Zeiss 510 confocal (60× objective).

Single-cell preparation and sorting

The SVZ and lesioned CC from 5 LPC injected or from 5 control 8–10 weeks old Gad67-GFP:Olig2-tdTomato mice were micro-dissected and pooled. SVZ were dissociated using the neural tissue dissociation kit from Miltenyi Biotec (Ref: 130-092-628) following manufacturer's instruction. Single-cell suspensions, previously stained with the Fixable Viability Dye eFluor 780 (Thermo Fisher 65-0865-14), were sorted on a 4-laser BD FACS Influx (BD Biosciences) equipped with a 100 μm nozzle. Single live cells were gated based on forward scatter, side scatter, trigger pulse width, and viability dye parameters. Autofluorescent cells were excluded based on their non-specific signal in the Amcyan channel. Cells were further gated as Gad67-GFP+, Olig2-Tomato+, or double positive. Single cells were FACS sorted into 96-well PCR plates containing 3 μL lysis buffer (10:1 mix of Resuspension Buffer and Lysis Enhancer from CellsDirect one-step qRT-PCR kit, Thermo Fisher 11753100). The index sorting mode was activated to record the different fluorescence levels of each sorted single-cell, allowing to verify the phenotype of each sorted cell specifically. After sorting, plates were covered with adhesive PCR film and immediately frozen on dry ice, then stored at −80°C until processing for single cell RNA-seq.

Library preparation and sequencing

Whole-transcriptome amplification and library construction were performed on single cells using the Smart-Seq2 protocol (Picelli et al., 2014). Lysed cells were thawed and subjected to retro-transcription using an Oligo(dT) primer and a template-switching oligo (TSO). Full-length cDNAs were then amplified by 23 cycles of PCR using the KAPA HiFi DNA polymerase (KAPA Biosystems). cDNAs were converted into uniquely bar-coded libraries using the Illumina Nextera XT sample preparation (Illumina) protocol. Each library was quantified and run on a bioanalyzer chip (Agilent) for quality check. High-quality libraries

were combined and sequenced with an Illumina HiSeq 4000. 184 single cells were profiled using this protocol.

QUANTIFICATION AND STATISTICAL ANALYSIS

On mouse brain sections

Cells were counted using the Zen software (Zeiss). All presented values are means ± S.E.M unless otherwise stated. Data were statistically processed with non-parametric Mann-Whitney test. $p < 0.05$ was considered as significant and $p < 0.01$ as highly significant.

On data analysis

All reads are available at the NCBI GEO : GSE130355). Reads were mapped to the isoform sequences of the *Mus musculus* ensemble release GRCm38 using kallisto (Bray et al., 2016) with the following parameters "kallisto quant–single-l 350-s 50-o-b 100". Gene levels were obtained by simply summing levels overall transcripts of a gene. Both matrices of counts and TPM were produced. All subsequent analyses were done using R (R Core Team, 2017). We selected 155 cells for which at least 20% of the sequenced reads mapped to the annotation, for a total of at least 200,000 mapped reads (all but three cells had at least 1,000,000 reads mapped). No effect of coverage was detected on our results (Figure S4C). We selected 3,422 genes that had a raw read count above 10 in at least 5 selected cells. Gene levels were then TMM normalized using the function normalizeBetweenArrays from the R package limma, so that the quantiles of the different samples were identical (Dillies et al., 2013).

Heatmaps were performed using the R function heatmap.2 (package gplots)

PCA analyses were done on the log transformed dataset (log10(normalized TPM+0.1)) using the command dudi.pca from the R package ade4 v1.7.11 with the following parameter "scale = F".

We performed two-way unsupervised clustering approach on the log transformed dataset (log10(normalized TPM+1)), after randomization of cell order, using BACKSPIN v3.5 (Zeisel et al., 2015) with the following parameters "-f 1000-t 100-g 5-r 0.2-c 2-d 4 –k 1.15".

Three cell populations were well recovered after biclustering: NB, NBL, OligNBL. The two remaining populations O and OL were recovered as a whole but the two subpopulations were not separated. We thus focused on the resulting 4 BACKSPIN clusters that recover NB, NBL, OligNBL and O + OL (Figure 2D). We selected cluster-specific markers as the 100 most enriched genes for each of the four clusters as previously described by *Marques* et al. (Marques et al., 2018). Briefly, enrichment was calculated for each gene using two variables that describe to which extent a gene is (1) specifically expressed in a unique cluster and (2) it is expressed in most cells of this cluster. Those variables are calculated as follows: (1) the ratio of cluster-specific expression over the expression in all cells (normalized to the cluster size) and (2) the proportion of cells in each cluster that harbor an expression above 1. The names of the resulting 400 markers are listed in Table S2 and their expressions are shown in Figure 2D.

Pseudo-temporal ordering was performed using the R package monocle v2.6.4 (Qiu et al., 2017) on the non-normalized, non log-transformed dataset of counts. Ordering was based on genes found as differentially expressed between, NB and O, using the function differentialGeneTest from monocle2.

Differential expression analysis was performed using the R package SCDE v2.6.0 (Kharchenko et al., 2014) on the non-normalized, non log-transformed dataset of counts. Genes were considered as differentially expressed if their Z score was above 2.58 (or below −2.58).

Meta-analyses of Figure 3 were performed on a merged dataset from three single cell RNA-seq studies: our study, cells from the Dulken et al. study (excluding the qNSCs that were less relevant to our analysis) (Dulken et al., 2017) and the cells from the Marques et al. study (Marques et al., 2018). We used the 400 marker genes obtained from the two-way unsupervised clustering analysis to minimize a dataset effect and because those genes are the most informative ones for our dataset (only 377 out of 400 genes harbored names compatible with the dataset from Dulken et al. and Marques et al. and were actually used). The obtained matrix was then TMM normalized. PCA described in Figure 3B was performed on the log (TPM+1)

transformed dataset. A similar analysis was performed on the full set of 8,346 genes and gave overall similar results but showed a stronger batch effect (Figure S6).

The comparison of molecular identity between different cell populations, including our OligNBL and the embryonic pri-OPC described by Weng et al. (2019), described in Figure 3E, was performed on a *meta*-dataset comprised 2877 cells: 152 aNSC and 29 NPC from Dulken et al. (2017); our 37 NB, 27 NBL and 40 OligNBL, 1,070 neuroblasts, 143 pri-OPC-GFAP, 738 pri-OPC-PDGFR, 90 OPC-GFAP and 340 OPC-PDGFR from Weng et al. (2019) and 201 OPC from Marques et al., (2018). Datasets were integrated using the Seurat package (all common 17,607 genes, 2,000 anchors and the 30 first axes after dimension reduction were used). Figure 3E was drawn using the DotPlot function from the Seurat package.

GO-term analyses were performed using the functional annotation clustering from DAVID 6.8, with the lowest classification stringency. GO-TERM were considered as significant when their Benjamini-Hochberg corrected p-values were <0.05.